Addressing the electrostatic component of protons binding to aquatic nanoparticles beyond the Non-Ideal Competitive Adsorption (NICA)-Donnan level: Theory and application to analysis of proton titration data for humic matter

José Paulo Pinheiro, Elise Rotureau, Jérôme F.L. Duval

Graphical Abstract

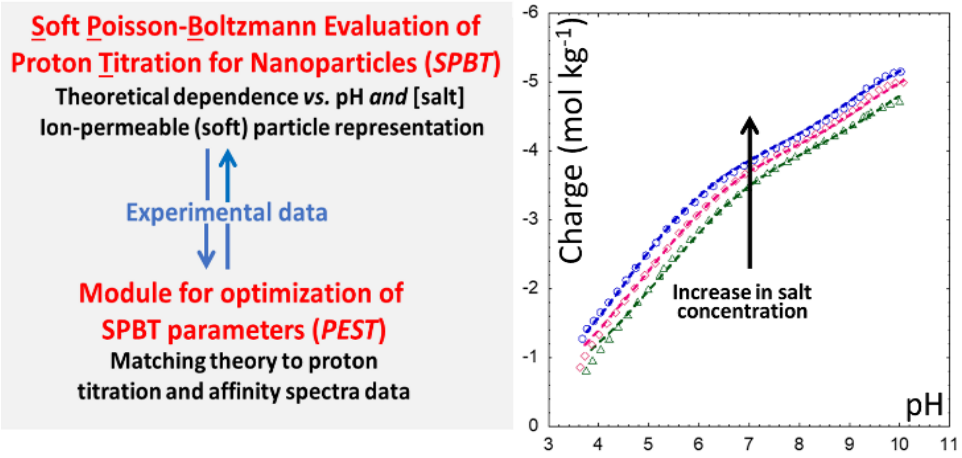

Addressing the electrostatic component of protons binding to aquatic nanoparticles beyond the Non-Ideal Competitive Adsorption (NICA)-Donnan level: theory and application to analysis of proton titration data for humic matter.

José Paulo Pinheiro,[1] Elise Rotureau,[1] Jérôme F. L. Duval[1,*]

[1] Université de Lorraine, CNRS, Laboratoire Interdisciplinaire des Environnements Continentaux (LIEC), UMR 7360, Vandoeuvre-lès-Nancy, F-54000, France.

[*] Corresponding author: jerome.duval@univ-lorraine.fr
Tel: 00 33 3 72 74 47 20

Abstract

Hypothesis.

Charge descriptors of aquatic nanoparticles (NPs) are evaluated from proton titration curves measured at different salt concentrations and routinely analysed by the Non-Ideal Competitive Adsorption-Donnan (NICAD) model. This model, however, suffers from approximations regarding particle electrostatics, which may bias particle charge estimation. Implementation of Poisson-Boltzmann (PB) theory within consistent treatment of NPs protolytic data is expected to address NICAD shortcomings.

Experiments.

An alternative to NICAD is elaborated on the basis of nonlinearized PB equation for soft particle electrostatics to properly unravel the electrostatic and chemical components of proton binding to NPs. A numerical package is developed for automated analysis of proton titration curves *and* proton affinity spectra at different salt concentrations. The performance of the method is illustrated for humic matter nanoparticles with different charge and size, and compared to that of NICAD.

Findings.

Unlike NICAD, PB-based treatment successfully reproduces particle charge dependence on pH for practical salt concentrations from the thin to thick electric double layer limit. Donnan representation in NICAD leads to moderate to dramatic misestimations of proton affinity and binding heterogeneity depending on particle size to Debye layer thickness ratio. Interpretation of NPs protolytic properties with PB theory further avoids adjustment of the 'particle Donnan volume' empirically introduced in NICAD.

Keywords. Poisson-Boltzmann theory, NICA-Donnan model, Particle electrostatics, Proton titration curves, Nanoparticles, Humic matter.

1. INTRODUCTION

Natural organic matter (NOM), the most important source of organic carbon on earth, is ubiquitous in soils and in aquatic ecosystems [1]. NOM refers to a broad spectrum of heterogeneous mixtures of macromolecules, nanoparticles and/or colloidal aggregates that differ in terms of physical and chemical properties including size, molecular weight, composition and charge [2]. The humic substances (HS), which represent the major NOM fraction, may be differentiated according to their solubility: the insoluble fraction, the humin, exists only in soils, whereas soluble fulvic and humic acids (hereafter denoted as FA and HA, respectively) are found in soils and natural waters [3]. Solubility of FA and HA further differs with respect to pH, with FA being fully soluble even under extreme acid conditions, and HA being soluble solely in weekly acidic and alkaline solutions [4]. Both FA and HA colloids are defined by nanometric dimensions with radius of *ca.* 1 nm and 2 to 10 nm [5], respectively. Accordingly, they are now generically termed as humic nanoparticles (HNPs in short) in literature.

The charge carried by HNPs strongly affects the mobility and the speciation of trace metal ions (M) in aquatic media. Indeed, it dramatically impacts on (i) the stability of HNPs-M complexes [6],[7]. (ii) the kinetics of the processes driving the formation and the dissociation of these complexes in solution [8],[9], and (iii) their lability, *i.e.* the extent to which complexes dissociate on the time scale of their diffusion toward M-consuming microorganisms [10],[11],[12]. The resulting connection between HNPs charge and metal bioavailability in aqueous environment motivates the need to address the electrostatic properties of HNPs at the proper quantitative level. The magnitude of the charge carried by HNPs inherently depends on solution pH and on background electrolyte concentration, both affecting the dissociation degree of the carboxylic and phenolic groups distributed throughout the HNPs volume [13]. In turn, the evaluation of HNPs charge properties from *e.g.* proton titration data analysis necessarily asks for an adequate differentiation between the chemical (intrinsic) and electrostatic components of the affinity of the protons for the HNPs carboxylic and phenolic sites [14]. Successful unravelling of these contributions is obviously tied to the robustness of the models in integrating the relevant electric double layer properties of HNPs, or, equivalently, the electrostatic potential distribution that is operational at the HNPs/solution interface.

So far, proton binding to HNPs has been mainly addressed from applications of the Windermere Humic Aqueous Model (WHAM) and of the Non-Ideal Competitive Adsorption (NICA) model developed in the 90's [15-18]. For the sake of conciseness, we refer the reader to Koopal *et al.* [19],[20] and Town *et al.* [7] for review and critical review of these modelling approaches. In their first attempt to integrate electrostatics within NICA formalism, de Wit *et al.* [21] interpreted proton titration data measured on various humic substances at different solution ionic strengths by means of the Poisson-Boltzmann (PB) theory applied to hard particles, *i.e.* particles impermeable to ions from the background electrolyte. Although such a PB-based modelling of humics electrostatic effects was reported to reproduce 'reasonably well' experimental titration data [21], a simpler but empirical electrostatic representation was proposed where the potential is *a priori* considered constant within the whole particle body *and* in a

surrounding solution volume adjusted to match proton titration data [13]. In its initial version, this 'Donnan-like' electrostatic model took the form of an equation involving 2 parameters describing empirically the dependence of a `Donnan volume´ on solution ionic strength [22], replaced later by an equation involving a single adjustable parameter [15]. It is this last version of the `Donnan-like representation´ that is integrated in the NICA-Donnan (NICAD) model and, except for some differences detailed elsewhere [7], in the WHAM model.

Even though NICA-Donnan modelling is largely adopted in metal speciation and proton binding studies involving HNPs [16] or other types of nanoparticles [19], there are severe inconsistencies in its account of particle electrostatics, as recently detailed by *e.g.* Town et *al.* [7]. Briefly, the spatial distribution of the electrostatic potential at the HNPs/solution interface adopted in NICAD violates the fundamental Poisson-Boltzmann formalism, a funding element of the classical DLVO theory [23]. Indeed, in the limit where particle radius well exceeds the electric Debye layer thickness in solution (a situation reached at sufficiently large electrolyte concentrations), the rigorous solution of the PB equation takes the form of a step-like potential profile where the potential is essentially constant inside the particle volume (this is the so-called Donnan potential) *and* zero outside: this is the *true* Donnan situation [24],[25],[26]. Accordingly, provided that medium salinity and particle size guarantee a correct application of the Donnan representation in line with the inequality $\kappa r_p >> 1$ with r_p the particle radius and $1/\kappa$ the Debye layer thickness, the Donnan volume cannot exceed the physical volume of the particles [7],[26]. This requirement is not respected by the NICAD model applied to HNPs [27]. In addition, within the NICAD modelling framework, the Donnan electrostatic picture is adopted regardless of the size of the particles considered and of the background electrolyte concentration, *i.e.* irrespectively of the value taken by κr_p. This implies that the Donnan representation is basically considered valid over the whole spectrum of electric double layer regimes, from the thick to the thin double layer extremes corresponding to $\kappa r_p << 1$ and $\kappa r_p >> 1$, respectively. Obviously, this assumption is incorrect, recalling that a Donnan potential profile is strictly operational under the only condition $\kappa r_p >> 1$ [7]. Given a radius of say 5 nm for HA particles, it is estimated that $\kappa r_p \sim 1.7$ to 5 in the range 10 mM to 100 mM electrolyte concentrations, respectively, this salinity range being commonly considered for HA proton titration experiments [28]. Therefore, under conditions where the electrostatic component is largest (*i.e.* at low κr_p) or, equivalently, when screening of particle electrostatics is least significant, the condition underlying the applicability of a Donnan potential representation is not respected, which makes inappropriate the use of Donnan-based modelling framework for HNPs [7].

The above shortcomings of the Donnan electrostatic model applied to HNPs are not new. Already in 1999, Avena *et al*. [27] explicitly recognized that "application of a simple Donnan model will only give results that are comparable to those obtained with the [PB] impermeable sphere model if the Donnan volumes used are larger than the specific volumes of the hydrated humics". In 2007, aware of the empirical nature of the adjustment of the 'particle Donnan volume' in NICAD, Companys *et al.* [29] proposed a

formulation of the Donnan volume on the basis of analytical solutions of Poisson-Boltzmann equation. The approach, however, excludes salinity conditions of practical interest where Donnan representation for HNPs is not applicable and it does not integrate the whole PB-based spatial distribution of the electrostatic potential. In 2005, Duval *et al.* [30] reported an electrokinetic analysis of HNPs particles over a large range of pH and electrolyte concentration conditions on the basis of an electro-hydrodynamic theory developed for the generic case of soft particles (*i.e.* permeable to ions from background electrolyte) [31] whose electrostatic properties were tackled at the non-linear PB level. The authors thereby demonstrated the inapplicability of the hard particles-representation for HNPs that display, instead, the characteristic electrokinetic signature of soft particles whose intraparticulate potential approaches the Donnan potential at sufficiently large κr_p. It is emphasized that the hard sphere-representation proposed earlier for HNPs [21] is not compatible with the establishment of a Donnan potential in the particle body: this potential follows indeed from the compensation of the *intraparticulate* HNPs structural charges by electrolyte ions that have been transferred from bulk solution to particle volume by conduction-diffusion transport. Finally, Saito *et al.* [32] revealed dramatic (sometimes exceeding 100 %) discrepancies between average HA particle potentials as determined by NICAD and that measured from fluorescence quenching. Instead, they evidenced better agreement with average potentials estimated on the basis of ion permeable-sphere model and with adopting an electrostatic particle representation that integrates the extraparticulate electric double layer contribution.

In view of the above elements, a sound physicochemical modelling of HNPs protolytic properties where particle electrostatics is tackled at the proper non-linear Poisson-Boltzmann level for soft spheres is still lacking in literature. In this work, we report such a formalism and we elaborate a numerical procedure able to handle automatically, consistently and simultaneously, the recovery of proton titration curves measured on HNPs of given size at different solution ionic strengths. These results are systematically compared to those published using empirical NICAD model, thereby clearly identifying the cases where application of NICAD is erroneous or approximate. The numerical package designed in this work is available on demand.

2. MATERIALS

Polydisperse HNPs samples may form aggregates depending on pH, medium salinity and nature of the cations in solution [33]. In turn, the evaluation of HNPs radius (r_p) and molar mass (M_w) from proton titration data modelling remains uncertain as the reliability of the obtained results necessarily depends on the way particle electrostatics is pictured, recalling that rigorous PB-based potential distribution at HNPs/solution interface intrinsically depends on particle size. To provide a clear comparison -free of the above uncertainties- between HNPs-protons binding properties derived following our approach and those obtained from NICAD, the analysis below is based on protons titration data sets collected on HNPs for which particle radius is measured by independent techniques and for which NICAD-based fitting parameters are explicitly provided in literature. Using such particle size estimation, we evaluated M_w of

the HNPs after exploiting M_w data reported for HNPs of composition similar than those considered in this work. As detailed below, this procedure constrains the modelling of protolytic titration data *versus* pH and electrolyte concentration and makes transparent the inherent electrostatic limits of NICAD model. In contrast, it advocates for the recourse to more rigorous soft PB theoretical framework. In line with the above elements, we selected five proton titration data sets published for HNPs with known particle radius, namely: the Ribeirão Preto Humic acid (FPHA)[34], Suwanee River Fulvic Acid (SRFA)[28], Laurentian Fulvic acid (LFA) [35] and the fulvic (Hf:FA) and humic acid (Hf:HA) from Sierra de Buio, Spain [36]. A detailed description of these HNPs, of their size measurement and of the estimation of their molar mass (**Table 1**) is provided in **Supporting Material** (**SM**, **section A** therein).

3. THEORY

The evaluation of HNP charge and protolytic properties is commonly carried out from the analysis of protons titration experiments performed in 1:1 electrolyte whose concentration is varied in the range 1 mM to 100 mM. The strategy thus consists in using the proton as a probe to explore the electrostatic-dependent charging behaviour of HNPs. In turn, pending proper theoretical treatment, titration data provide the desired relevant electrostatic descriptors and charge of HNPs as a function of pH and electrolyte concentration.

3.1. Electrostatic and chemical descriptors of HNPs. The total charge Q^0 carried by a single HNP and accessible from titration experiments may be expressed as the integral over the intraparticulate volume of the density $\rho_0^{(s)}$ (in C m^{-3}) of net charges stemming from the dissociation of the structural carboxylic and phenolic groups distributed throughout the HNPs volume:

$$Q^0(\mathrm{pH}, c_{\mathrm{elec}}^{\infty}) = \frac{4\pi}{FV_p}\int_0^{r_p} \rho_0^{(s)}(r, \mathrm{pH}, c_{\mathrm{elec}}^{\infty}) r^2 \mathrm{d}r \quad (1)$$

where $V_p = 4\pi r_p^3/3$ is the volume of an individual HNP (m^3), r is the radial coordinate with the particle centre positioned at r=0, r_p is the particle radius, F is the Faraday and Q^0 is expressed as a concentration of monovalent charges per unit HNPs volume (mol m^{-3}). Eq 1 makes explicit that Q^0 and $\rho_0^{(s)}$ both depend on solution pH and on the background electrolyte concentration denoted as $c_{\mathrm{elec}}^{\infty}$. The charge density $\rho_0^{(s)}$ is determined by the local concentration of protons within the HNP body which itself depends on the potential profile $\psi(r)$. For the sake of convenience, we introduce the dimensionless local electrostatic potential defined by $y(r) = zF\psi(r)/RT$ where z is the valence of the z:z background electrolyte (z=1 under commonly adopted titration experiment conditions). The radial dependence of $y(r)$ is governed by the Poisson-Boltzmann (PB) equation where contributions from ***both*** (immobile) structural charges carried by HNPs ***and*** (mobile) ions from the background electrolyte are accounted for. After straightforward arrangements, the dimensionless PB equation applicable to soft HNPs particles reads as[37][‡]

[‡] There is a typo error in eq 3 of ref. 37 where a minus sign is missing in front of the charge density term.

$$\frac{d^2y(\tilde{r})}{d\tilde{r}^2}+\frac{2}{\tilde{r}}\frac{dy(\tilde{r})}{d\tilde{r}}-\sinh[y(\tilde{r})]=-\frac{\rho_0^{(s)}(\tilde{r},\mathrm{pH},c_{\mathrm{elec}}^{\infty})}{2Fzc_{\mathrm{elec}}^{\infty}} \quad (2)$$

where $\tilde{r}$ is the dimensionless radial position defined by $\tilde{r}=\kappa r$ with κ the reciprocal Debye length given by

$$\kappa=\sqrt{2F^2z^2c_{\mathrm{elec}}^{\infty}/(RT\epsilon_0\epsilon_r)} \quad (3)$$

with ϵ_0 the dielectric permittivity of vacuum and ϵ_r the relative dielectric permittivity of the medium. Eq 3 tacitly implies that the contribution of the protons and hydroxyl ions to the total solution ionic strength is not significant, which is legitimate under the pH and 1:1 electrolyte concentration conditions adopted in this work (and in many reports from literature [28]). Relaxing this condition is straightforward pending replacement (i) of eq 3 by $\kappa=\sqrt{\sum_{j=1}^{N}F^2z_j^2c_j^{\infty}/(RT\epsilon_0\epsilon_r)}$ where the index *j* runs over all types of ions with bulk concentration c_j^{∞} present in solution, including H^+ and OH^-, and (ii) modification of the sinh term in eq 2 along the lines given elsewhere [38]. In addition, the current version of the program makes it possible the analysis of measurements performed in 2:1 electrolytes based on a proper transformation of eq 2 along the lines detailed in [6] (see eqs S1-S2 therein). Application of the formalism to other mixtures of electrolytes is further possible pending differentiation in eq 2 between the various Boltzmann terms associated with the respective contributions of the mobile ions to the overall charge of the extra- and intra-particulate electric double layers. Last, the program allows, if required, the extraction of the Boltzmann factor for proton accumulation (or that of any ions present in the electrolyte) within the overall body of the particle. This is done by spatial integration of the relevant local Boltzmann factor, as detailed in [6]. Also, if required, the Boltzmann factor pertaining to ion accumulation in the extraparticulate double layer can be easily retrieved upon proper setting of the limits of the corresponding spatial integration.

The boundary conditions associated to eq 1 are provided by

$$y(\tilde{r}\to\infty)=0\ ;\ \left.\frac{dy(\tilde{r})}{d\tilde{r}}\right|_{\tilde{r}=0}=0 \quad (4a,b)$$

where eq 4a reflects electroneutrality condition in bulk electrolyte solution and eq 4b results from symmetry of the potential profile at the particle centre. For the sake of demonstration, the developments below are illustrated for HNPs particle but the formalism remains valid for any particle type pending implementation of the relevant (Dirichlet- or Neumann-type of) electrostatic boundaries [39] and consideration of the proper number of structural charges type (set to 2 for HNPs) [40].

Under given pH and solution ionic strength conditions, the characteristic potential distribution $y(\tilde{r})$ derived from eqs 1-2 takes the form of a bell shape with a maximum reached at the particle center, and it decreases gradually to zero value at few $1/\kappa$ distances far from the particle surface located at $r=r_p$ [37]. In the limit $\kappa r_p >> 1$, the electrostatic Donnan situation is achieved with $y(r\le r_p)=y_D$ and $y(r>r_p)=0$ where y_D is the dimensionless Donnan potential [7]. It is emphasized that the local pH inside the HNPs volume depends on position *r* and thus differs from the solution pH to an extent that depends on the particle charge, or equivalently, on the magnitude of the intraparticulate potential.

The raw data Q obtained from proton titration experiments are classically expressed in equivalent concentration of monovalent charges per mass of titrated HNPs (*i.e.* Q is in mol kg^{-1}). Q is then related to the volume charge density Q^0 (mol m^{-3}) of a single HNP particle (eq 1) according to

$$Q = Q^0 V_p N_A / M_W = Q^0 v_p \quad (5)$$

where N_A is the Avogadro number, M_W (kg mol^{-1}) is the molar mass of the considered HNP material, and $v_p = V_p N_A / M_W$ is the specific volume of HNP (in m^3 kg^{-1}). The conversion of Q^0 to a charge expressed in standard experimental unit (mol kg^{-1}) therefore requires knowledge of the particle radius r_p and of the molecular weight M_W, or of the only specific volume v_p. This conversion is systematically required because PB-based electrostatics of particles does not depend on the total amount of charges carried by the particles but, instead, by their volume density of charges.

The structural charges carried by HNPs originate from the (de)protonation of carboxylic and phenolic groups. Due to the intrinsic chemical heterogeneity of HNP material, equilibrium protonation constants are classically modelled as continuous distributions [41] involving mean protonation constants denoted as $\overline{K}_{a1}$ and $\overline{K}_{a2}$ for the carboxylic and phenolic groups, respectively, and the distribution width m_{H1} and m_{H2}. The later reflects the chemical heterogeneity of the carboxylic and phenolic binding sites throughout HNPs due to differences in their molecular environments. The limits m_{H1}=m_{H2}=1 apply to ideal situations where HNP composition is homogeneous. The local structural charge density, $\rho_0^{(s)}(r, \mathrm{pH}, c_{\mathrm{elec}}^{\infty})$ involved in eqs 1-2 is then provided by

$$\rho_0^{(s)}(r, \mathrm{pH}, c_{\mathrm{elec}}^{\infty}) = \frac{\rho_{\mathrm{maxH1}}^{(s)}}{1+10^{m_{\mathrm{H1}}(\mathrm{p}\overline{K}_{a1}-\mathrm{pH})}\exp[-m_{\mathrm{H1}}y(\tilde{r})]} + \frac{\rho_{\mathrm{maxH2}}^{(s)}}{1+10^{m_{\mathrm{H2}}(\mathrm{p}\overline{K}_{a2}-\mathrm{pH})}\exp[-m_{\mathrm{H2}}y(\tilde{r})]} \quad (6)$$

where $\rho_{\mathrm{maxH1}}^{(s)}$ and $\rho_{\mathrm{maxH2}}^{(s)}$ are the maximum densities of structural charges (mol m^{-3}) achieved under pH conditions where all carboxylic and phenolic sites are fully deprotonated, respectively. $\rho_{\mathrm{maxH1}}^{(s)}$ and $\rho_{\mathrm{maxH2}}^{(s)}$ may be transformed in mol kg^{-1}, by multiplication by v_p, resulting in Q_{maxH1} and Q_{maxH2}, respectively. The set of eqs 1-6 fully determines the dependence of the searched charge Q on pH and ionic strength. A Fortran program (named **SPBT** for **S**oft **P**oisson **B**oltzmann-based **T**itration) was developed to compute eqs 1-6. In particular, the solution of eq 2 was derived according to the numerical strategy employed elsewhere [42] using Fortran COLSYS subroutine [43] which approximates the solution through spline-collocation at Gaussian nodes and selects mesh subdivision following an auto-adaptative strategy. This algorithm has already been proven extremely efficient for evaluation of *e.g.* complex soft particle electrokinetics [44] and soft macrosurface electrohydrodynamics [45]. The one-component NICA equation commonly adopted for proton titration analysis is a Langmuir-Freundlich equation that involves, similarly to eq 6, the protolytic parameters $\rho_{\mathrm{maxH1}}^{(s)}$, $\rho_{\mathrm{maxH2}}^{(s)}$ (or Q_{maxH1} and Q_{maxH2}), $\overline{K}_{a1}$, $\overline{K}_{a2}$, m_{H1} and m_{H2} (see details of NICAD modelling in **SM**, **section B**). The electrostatic component of this NICA equation is tackled *via* a Donnan-like representation of the potential profile inside the particle body *and* in its aqueous surrounding, as commented in the Introduction section and further detailed in **SM**, **section B**.

3.2. Fitting proton titration data to theory: strategy. The theoretical framework provided by eqs 1-6 involves 8 parameters that must be consistently adjusted to reproduce proton titration data collected at different solution ionic strengths, namely r_p, M_w, $\rho^{(s)}_{\mathrm{maxH1}}$, $\rho^{(s)}_{\mathrm{maxH2}}$ (or Q_{maxH1} and Q_{maxH2}), $\overline{K}_{a1}$, $\overline{K}_{a2}$, m_{H1} and m_{H2}, all of them being independent of the solution ionic strength provided that particles do not significantly swell with varying pH or $c^{\infty}_{\mathrm{elec}}$, which is the case for *e.g.* FA and HA (see related discussion in the next section) [7],[46]. As the range of r_p and M_w values is known (**Table 1**), this number basically reduces to 6, which is consistent with the conclusion by Lenoir and Manceau [47] who evidenced, *via* Principal Component Analysis (PCA) of proton titration data collected on a large series of fulvic and humic samples, that only 6 independent parameters could be adjusted to reproduce experiments with least-square minimization. The analysis of proton titration data using the current version of NICAD requires one additional parameter to be adjusted. This parameter, termed *b*, connects empirically the 'particle Donnan volume' V_D (erroneously allowed to exceed V_p) where the potential is considered *a priori* constant, to the logarithm of the solution ionic strength, log *I*. Lenoir *et al.* [47] argued that using NICAD, "the total covariance of the system cannot be reduced by measuring titration data at various ionic strengths because log *I* is correlated to log V_D". This observation mirrors the failure of NICAD in establishing at the correct PB level the connection between potential profiles at the HNPs/solution interface and medium salinity. Janot *et al.* [35] compared unconstrained and constrained proton procedures for titration data fitting with use of NICAD. They concluded that different sets of model parameters derived with different procedures could lead to similar quality of data fit, thereby questioning again the physical relevance of the obtained model parameters. Another important aspect is that the lack of obvious inflection points in the proton titration curves implies that the quality of the theoretical recovery of the titration data, regardless of the funding modelling approximations, may depend on the initial estimates of the adjusted parameters, which in turn conditions the performance of the algorithm to converge to a solution with minimisation of residuals [48]. Accordingly, to obtain more reliable information on HNPs charge and electrostatic properties from confrontation between experiments and theory, the fitting procedure we adopt, detailed in the next section, considers *simultaneously* the reconstruction of the proton titration data (*Q vs.* pH) *and* that of its first derivative with respect to pH (d*Q*/dpH *vs.* pH), the so-called proton affinity spectrum.

3.3. Procedure for proton titration data reconstruction. The parameters r_p, M_w, Q_{maxH1}, Q_{maxH2}, $\overline{K}_{a1}$, $\overline{K}_{a2}$, m_{H1} and m_{H2} were optimized to reproduce the raw proton titration data and the associated affinity spectra by coupling our home-made Fortran program SPBT with **PEST**, an open source software for adjustment and estimation [49] of parameters by confrontation of theoretical models to experimental data. The minimization procedure adopted in PEST for fitting theory to data is based on Gauss-Marquardt-Levenberg algorithm which minimizes the weighted sum Σ of squared differences between model-generated data (supplied here by SPBT) and corresponding experimental measurements. **Figure S1** in **SM** (**section C**) summarizes the key steps of the proton titration data treatment by the coupled SPBT-PEST

codes, which includes the estimations of sound initial guessed values for the chemical parameters Q_{maxH1}, Q_{maxH2}, m_{H1}, m_{H2}, $\overline{K}_{a1}$ and $\overline{K}_{a2}$ (**SM**, **Figure S2, section D**) as well as refinement of measured r_{p} and M_{w}. Optimization of r_{p} and M_{w} at one side and Q_{maxH1}, Q_{maxH2}, m_{H1}, m_{H2}, $\overline{K}_{a1}$ and $\overline{K}_{a2}$ at the other is performed according to a two-step process detailed in **Figure S1**. The reader is referred to **SM** (**section C**) for exhaustive details of the procedure driving the iterative dialog between PEST (in charge of the generating parameters and confronting experimental prediction to experimental data) with SPBT that computes (*Q vs.* pH and *I*) and (d*Q*/dpH *vs.* pH and *I*) data for given set of parameters.

In the next section, we discuss the performance of SPBT-PEST in reproducing the *Q* and d*Q*/dpH *vs.* pH data measured at different background electrolyte concentrations for the HNPs samples listed in **Table 1**. We further compare the corresponding sets of optimized parameters with those derived by NICAD-based modelling and reported in literature for FPHA [34], SRFA [28], LFA [35], Hf:FA [36] and Hf:HA [36] particles.

4. RESULTS AND DISCUSSION

4.1. Comparison between HNPs specific volume derived from SPBT-PEST and Donnan volume estimated from NICAD modelling

As detailed in the theoretical section, the particle radius r_{p} and molecular weight M_W can be used to compute the particle specific volume v_p ($m^3\ kg^{-1}$). **Table 1** collects r_{p}, M_W and v_p obtained from SPBT-PEST analysis of the proton titration data measured at different solution ionic strengths for the various HNPs of interest. For the sake of comparison, **Table 1** further reports the NICAD-based Donnan Volume V_{D} (also expressed in $m^3\ kg^{-1}$) estimated for the various HNPs types considered on the basis of NICAD model parameters published in literature**.**

Table 1: Comparison between HNPs specific volumes v_p derived in this work and model-generated Donnan volume V_{D} computed from the parameters reported in literature for NICAD modelling. Eq S3 and eq S4 given in **SM** specify the way V_{D} was estimated, *i.e.* either *via* the two-parameter (α, β) dependent or the one-parameter (b) dependent NICAD empirical equations that relates V_{D} to the logarithm of ionic strength. Initial estimates (superscript i in the Table) and refined values (superscript ii) of particle size r_{p} and molecular weight M_{w} by SPBT-PEST are further indicated. Numbers between brackets correspond to κr_{p} values, recalling that Donnan potential-representation is strictly applicable for κr_{p} >>1.

HNPs type	r_{p} ($\times 10^{-9}$ m)	M_{w} (kg mol^{-1})	v_p ($m^3\ kg^{-1}$)	Donnan fitting parameters	Model-generated Donnan volume V_{D} ($m^3\ kg^{-1}$)		
				α,β for eq. S3 or b for eq. S4	100 mM	10 mM	1 mM
FPHA [34]	3.1 to 5.9*,[i] 5.0[ii]	19.2 to 23[i] 23 [ii]	0.0137	α=0.60±0.32 β=-0.27±0.05	0.0074 (5.20)	0.0138 (1.64)	0.0257 (0.52)
SRFA [28]	0.6 to 1.05 [i] 0.6[ii]	0.5 to 1.5[i] 0.545 [ii]	0.0010	b=0.87	0.0055 (0.60)	0.0407 (0.20)	0.3020 (0.06)

LFA [35]	1.9 to 3.6[i] 3.6[ii]	5.5 to 11[i] 10 [ii]	0.0118	b=0.35 ± 0.02	0.0004 (3.74)	0.0009 (1.18)	0.0019 (0.37)
				α=0.93±0.20 β=-0.27±0.05	0.0158 (3.74)	0.0295 (1.18)	0.0550 (0.37)
Hf:FA [36]	0.75 to 1.0[i] 1.0[ii]	0.5 to 1.5[i] 0.9 [ii]	0.0028	b=0.43	0.0007 (1.04)	0.0019 (0.33)	0.0052 (0.10)
Hf:HA [36]	0.75 to 1.0[i] 1.0[ii]	1.0 to 3.0[i] 1.8 [ii]	0.0014	b=0.34	0.0005 (1.04)	0.0010 (0.33)	0.0023 (0.10)

*Determined in this work by Scanned Stripping Chronopotentiometry (SSCP), see details in **SM** (**section A**, therein).

The Donnan volume V_D significantly increases with decreasing solution ionic strength I. This dependence of V_D on I, systematically observed with NICAD modelling regardless of sample types [19], has been motivated by viscosity measurements and argued to stem from particle swelling [50]. However, as discussed by Town *et al.*,[7] this justification is questionable because it ignores the influence of primary and secondary electroviscous effects that originate from particle electric double layer interactions and interparticulate electrohydrodynamic interactions. These effects, in turn, can lead to substantial variations in the viscosity of particle dispersions with pH and ionic strength even under *constant* particle size conditions [51],[52],[53]. Besides, may the particle size (and thus V_D) increases significantly with decreasing I, one would anticipate a strong dependence of V_D with pH, similarly to that observed for *e.g.* responsive PNIPAM particles [54], essentially because the driving electrostatic force for particle swelling depends on particle charge and thus on both I *and* pH. In contradiction to this anticipation, V_D is considered constant with pH in NICAD modelling. Last, for both HA and FA of soil and aquatic origins, particle size measurements performed with different techniques [7],[55],[56] show that there is no significant ionic strength- nor pH- dependent swelling/contraction of the particles in aqueous dispersions (the argument excludes *extreme* pH and I conditions where particles aggregation may take place). These elements highlight the empirical *ad hoc* fitting/calibration of V_D for every salt concentration tested. In addition, for many of the situations considered in **Table 1**, V_D exceeds v_p. This basically comes to position particle structural charges within a volume that exceeds the physical volume of the particle, which is inconsistent from an electrostatic point of view. Within the PB framework adopted in SPBT-PEST analysis of proton titration data and proton affinity spectrum, the HNPs specific volume v_p is independent of solution pH and ionic strength and, accordingly, it does not suffer from the inconsistencies of V_D estimates listed above. Last, it is clear that for most of the salinity and particle size conditions examined, the $\kappa r_p >> 1$ condition required for rigorous application of a Donnan representation of the electrostatic potential distribution at HNPs/solution interface is not satisfied (see **Table 1**), which further questions the physical meaning of the NICAD framework applied under such conditions.

4.2. Performance of SPBT-PEST in recovering proton titration and affinity spectrum data.

Figures 1 and **2** report the SPBT-PEST theoretical analyses of the proton titration and affinity spectrum data measured for FPHA and SRFA at different $NaNO_3$ electrolyte concentrations, respectively, and the corresponding adopted model parameter values are listed in **Table 2** together with their statistical dispersion evaluated by PEST. For the sake of conciseness, reconstruction of data pertaining to LFA, Hf:FA and Hf:HA are given in **SM** (**section E**, **Figures S3-S5**) and corresponding model parameters are provided in **Table 2**.

Figure 1A shows a good agreement between titration experiments and SPBT-based theory for FPHA particles. In particular, the analysis reproduces with accuracy the electrostatic component of the proton binding to the particles, which is materialized by the correct positioning of the theoretical curves with varying background electrolyte concentration. This successful match between theory and experiments does not suffer from *ad hoc* adjustment of particle size and it intrinsically integrates the way intraparticulate ***and*** extraparticulate electrostatic potential distributions are modified with varying particle size and electrolyte concentration, features that are not shared by the empirical NICAD modelling framework. It is further emphasized that data treatment on the basis of SPB-PEST is significantly more constrained than that performed with using NICAD as the former, unlike the latter, considers simultaneous analysis of proton titration *and* affinity spectrum.

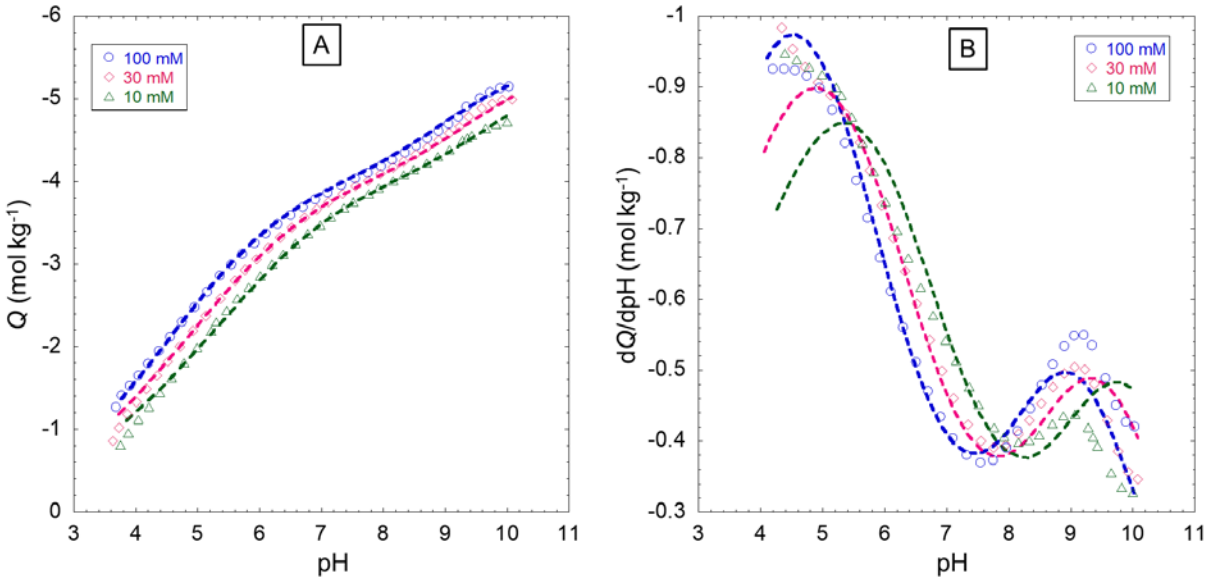

Figure 1: Proton titration curves for FPHA (A) and corresponding proton affinity spectra (B) collected at three $NaNO_3$ electrolyte concentrations: 10 mM (Δ), 30 mM (◊) and 100 mM (o). Symbols: measurements. Dotted lines: SPBT-PEST modelling results. Model parameters are listed in **Tables 1-2**. The charge is expressed in moles of equivalent charges per kg of FPHA material.

Table 2: SPBT-PEST optimized values of the chemical parameters involved in the Langmuir-Freundlich equation (eq 6) for the various HNPs types considered in this work. Indicated dispersions of the parameters correspond to the 95% confidence interval provided by PEST. The parameters are retrieved from SPBT-PEST and NICAD modelling of the proton titration curves measured at different salt reconstructions and reported in **Figures S6-S10** for the five HNPs samples of interest. SPBT-PEST and NICAD theoretical reconstructions of these proton titration data *versus* pH and salt concentration are also provided in **Figures S6-S10**.

HNPs type	*Model*	Q_{maxH1} (mol kg^{-1})	log $\overline{K}_{a1}$	m_{H1}	Q_{maxH2} (mol kg^{-1})	log $\overline{K}_{a2}$	m_{H2}
FPHA	SPBT-PEST	4.08 ± 0.02	4.26 ± 0.02	0.46 ± 0.01	1.39 ± 0.07	8.57 ± 0.09	0.59 ± 0.03
	NICAD/eq.S3 [34]	3.18 ± 0.92	3.65 ± 0.23	0.66	3.02 ± 2.4	8.07 ± 0.77	0.29
SRFA	SPBT-PEST	5.47 ± 0.06	3.20 ± 0.02	0.52 ± 0.01	1.0 ± 0.4	7.8 ± 0.2	0.5 ± 0.2
	NICAD/eq.S4 [28]	5.55	3.01	0.42	NA*	NA*	NA*
LFA	SPBT-PEST	3.79 ± 0.12	3.94 ± 0.03	0.52 ± 0.02	4.94 ± 0.10	8.5 ± 0.2	0.27 ± 0.01
	NICAD/eq.S4 [35]	2.8 ± 1.2	2.5 ± 0.2	0.62 ± 0.17	7.4 ± 2.5	7.4 ± 0.7	0.18 ± 0.06
	NICAD/eq.S3 [35]	5.1 ± 0.0	4.1 ± 0.1	0.41 ± 0.01	2.8 ± 0.0	8.6 ± 0.1	0.46 ± 0.02
Hf:FA	SPBT-PEST	4.35 ± 0.09	3.81 ± 0.01	0.91 ± 0.02	1.75 ± 0.06	7.1 ± 0.3	0.33 ± 0.01
	NICAD/eq.S4 [36]	5.0±0.01	2.29±0.01	0.44	0.94 ±0.03	6.85±0.02	0.59
Hf:HA	SPBT-PEST	3.00 ± 0.05	4.40 ± 0.02	0.83 ± 0.03	1.3 ± 0.2	7.5 ± 0.2	0.49 ± 0.05
	NICAD/eq.S4 [36]	3.44± 0.02	3.35 ± 0.01	0.46	0.64 ± 0.04	6.68 ± 0.03	0.88

NA (not available)*: NICAD fit was carried out only for site 1 type (*i.e.* carboxylic) due to the experimental data that cover a reduced range of pH values (see Fig. 2)

Figure 1B shows some discrepancies between SPBT-PEST outcome and proton affinity spectrum data especially at low and high pH values. In the low pH range, suspensions of HNPs are indeed more prone to aggregation due to significant lowering of the charge carried by the particles [57], while pH measurements by glass membrane electrodes become unstable at sufficiently high pH due to unbalanced competition between protons and sodium ions from background electrolyte solution [58]. In addition to these unavoidable experimental difficulties, the estimation of d*Q*/dpH may be subject to significant error as tiny deviations of the dependence of *Q* on pH compared to a smooth trajectory, may lead to significant changes in estimated d*Q*/dpH.

The titration data collected from literature for SRFA particles relate to pH lower than 7.5 (**Figure 2A**). Accordingly, the chemical parameter values retrieved for the phenolic sites should be considered with caution as their dissociation is not significant in the pH range examined, which is supported by the absence of a second peak in the affinity spectrum (**Figure 2B**). The experimental titration data at 1 and 10 mM $NaNO_3$ are anomalously superimposed for this HNPs sample type, which may be explained by an inaccurate positioning of the experimental curves by Milne *et al*. [28]. The SRFA titration curve is marked by a steep increase of the particle charge with increasing pH from 3 to 6, similarly to that observed for a weak acid: this feature is consistent with the low log $\overline{K}_{a1}$ value of 3.2 derived for the carboxylic groups.

The lack of data at higher pH values is reflected by the large errors made in the estimation of the optimised parameters pertaining to the phenolic sites, particularly for Q_{maxH2} and m_{H2} (**Table 2**). The variations of the proton affinity spectrum at low pH are better defined for the sub-nanometric SRFA particles than those measured for the larger FPHA particles (**Figure 1B**), which supports that particles aggregation - facilitated with increasing particle size [57]- likely affects data quality in this pH range.

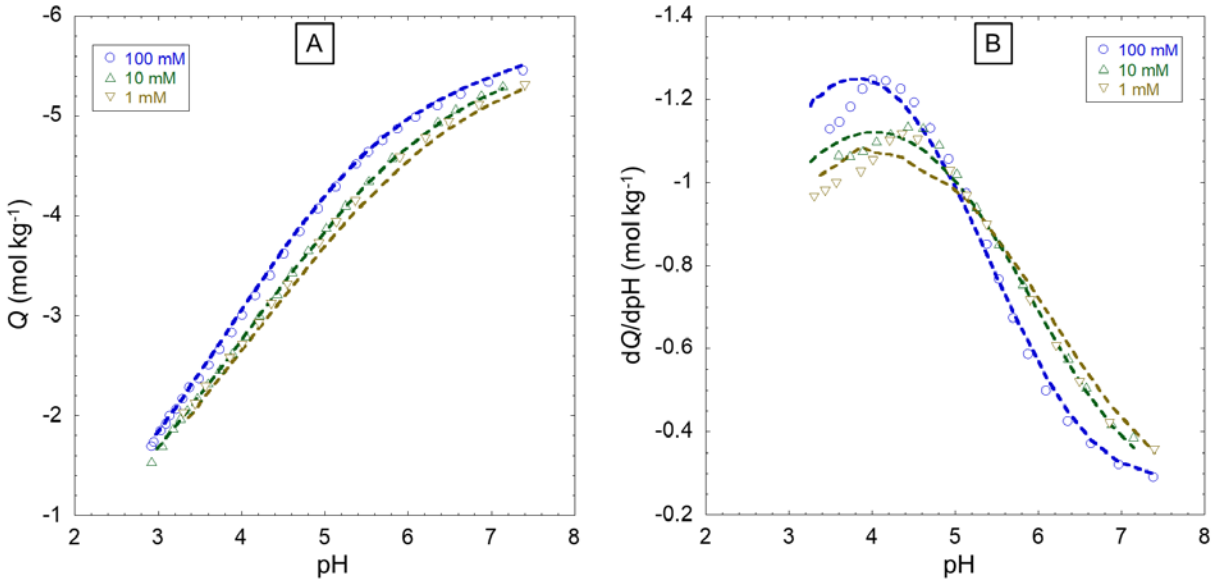

Figure 2: Proton titration curves for SRFA (A) and corresponding proton affinity spectra (B) collected at three $NaNO_3$ electrolyte concentrations (indicated). Symbols: measurements. Dotted lines: SPBT-PEST modelling results. Model parameters are given in **Tables 1-2**. The charge is expressed in moles of equivalent charges per kg of SRFA material.

The experimental results collected for LFA particles are of good quality up to pH 8 (**SM**, **Figure S3**) but some suspicious changes in the measurements can be observed at larger pH, especially at 30 mM ionic strength, which is particularly evidenced by inspection of the proton affinity spectra. The SPBT-PEST reconstruction of the LFA proton titration data is satisfactory for all electrolyte concentrations conditions examined, which contrasts with the theoretical quality of the corresponding proton affinity spectra. As mentioned above, this is so because the computation of the derivative dQ/dpH is very sensitive to changes of Q with pH, even very small. The results derived for Hf:FA (**SM**, **Figure S4**) and Hf:HA (**SM**, **Figure S5**) are quite similar, with the noticeable result that chemical heterogeneity viewed by the prism of m_{H1} is modest for both samples (**Table 2**). A difference is that carboxylic sites fraction is more significant in Hf:FA and associated log $\overline{K}_{a1}$ is significantly lower than that for Hf:HA. Inspection of **Figures S4-S5** reveals that SPBT-based theory slightly overestimates experiments at low electrolyte concentrations (10 mM and 5 mM). Whereas it is difficult to provide firm explanations of such differences for Hf:FA and Hf:HA samples, possible origins of the mismatch between experiments and theory (mismatch that is more pronounced with NICAD-based modelling, see **SM**, **section F**) can be advanced: the effectiveness of the protocol for separating the sub-nanometric fulvic and humic fractions in these samples, an approximate

positioning of the experimental titration data at 5 and 10 mM, or the occurrence of physico-chemical reactions affecting the structure of the particles at sufficiently low medium salinity.

4.3. Comparison between protolytic chemical parameters of HNPs retrieved by SPBT-PEST and NICAD

As discussed above, the Donnan-like representation considered within NICAD modelling does not provide a consistent picture of the soft HNPs electrostatic properties. It is then of importance to address how the inconsistency of this unconstrained, empirical modelling approach is reflected in the NICAD-derived protolytic chemical parameters. For that purpose, **Table 2** collect Q_{maxH1}, Q_{maxH2}, m_{H1}, m_{H2}, $\overline{K}_{a1}$ and $\overline{K}_{a2}$ derived by NICAD and provided in the literature for the samples of interest, to be compared with the values obtained by SPBT-PEST. In addition, for the sake of completeness we report in **Figures S6-S10 (SM**, **section F)** the NICAD-based fitting of the proton titration curves for all HNPs listed in **Table 1** together with those obtained by SPBT-PEST. Briefly, data reconstruction quality by NICAD for the largest FPHA and LFA HNPs considered in this work is quite comparable for all examined ionic strengths to that achieved by SPBT-PEST, whereas it is significantly worse for all other HNPs defined by lower r_{p}. This conforms qualitatively with the fact that the NICAD assumption of a constant intraparticulate potential is best verified for large particles, more prone to satisfy the criterion $\kappa r_{\mathrm{p}} >> 1$ under given medium salinity conditions. Surprisingly, NICAD manages to provide a reasonable estimates of proton titration data for FPHA and LFA at low ionic strengths where Donnan criterion is not satisfied (see **Table 1**): it does so, however, at the cost of unrealistic adjustment of V_{D} already invoked by Town *et al*. [7] and Lenoir *et al*. [48] Further comparison between $\overline{K}_{a1,2}$ derived by NICAD and SPBT-PEST (**Table 2**) shows important differences, especially for carboxylic groups for which this difference may amount to more than an order magnitude. This difference is most important for Hf:FA and Hf:HA samples for which NICAD modelling is inappropriate (**SM**, **Figures S9-S10**), and it remains marginal for SRFA and LFA despite of the corresponding poor NICAD-based titration data reconstruction (**SM**, **Figure S7**) and/or the inapplicability of the Donnan criterion over the whole range of solution ionic strength considered (**Table 1**). For Hf:FA, the $\log \overline{K}_{a1}$ (2.29±0.01) obtained by NICAD is further anomalously low for carboxylic acid and it compares to the first proton dissociation constant of a stronger acid like phosphoric acid (pK_{a}=2.12) [59]. As a matter of fact, this suspicious $\log \overline{K}_{a1}$ value just mirrors the attempt of NICAD to balance its physically erroneous description of particle electrostatics *via* artificial adjustment of V_{D}. The reader is referred to **Table 1** and **Table 2** to appreciate the over- or under-estimation of the quantities Q_{maxH1}, Q_{maxH2}, m_{H1} and m_{H2} by NICAD as compared to those derived by SPBT-PEST. It is worth mentioning that huge differences of these quantities (some approaching or exceeding 100%, see **Table 2** for LFA data) are obtained by NICAD depending on the nature of the V_{D}-$\log I$ relationship adopted (either one or two-parameters dependent relation, see eqs S3 and S4 in **SM**, respectively). This observation, further supported by the large differences in V_{D} (see **Table 1** for LFA) simply reflects, again,

the phenomenological nature of the NICAD fitting exercise that is based on an electrostatic representation unsupported by the particle size-dependent intra- and extra-particulate spatial distributions governed by PB formalism for soft particles. Even with application of NICAD model under conditions where its founding electrostatic approximation is not verified, proton titration data reconstruction can be more or less 'satisfactory': this underpins the empirical nature of NICAD-based fitting of such data. Unsurprisingly, adopting eq S3 provides better reconstruction of proton titration data than with using eq S4 simply because the degree of parameters adjustment offered to the user is larger with the former equation.

5. CONCLUSIONS

Since the 90's when the first versions of the Non-Ideal Competitive Adsorption-Donnan model (NICAD) were developed [15-18], the community of environmental physical chemists has largely employed the NICAD model to estimate the chemical charge carried by aquatic nanoparticles from proton titration data measured at different salt concentrations [15-18,21,22,28,34-36,40,48,60-62]. Accurate knowledge of the charge of these particles is fundamental as *e.g.* it largely contributes to define the fate, speciation and bioavailability of charged contaminants like metals in the aqueous compartments of ecosystems. In particular, there is a large amount of literature data reporting analysis by NICA-Donnan or related models, of the protolytic properties of humic matter nanoparticles (HNPs) commonly viewed as model surrogates for organic matter particles in aquatic environments or soils [18,19,21,22,28,34-36,47,48,50,60-62]. For the sake of illustration, ecotoxicologists often employ HNPs as model systems to analyse the speciation of hazardous metals in dispersions of charged colloids and the implications thereof in terms of identification of the toxic metal forms towards living organisms (*e.g.* plants, bacteria, or algae) [63].

Despite of its popularity, NICA-Donnan suffers from severe approximations on the way particle electrostatics is implemented, recalling that estimation of the charge carried by any colloidal particles necessarily requires a proper formulation of the electrostatic component of the binding of the charge-determining ions (protons) to the ionogenic sites distributed at the particle surface and/or in the particle body volume. Namely, NICAD assumes the applicability of Donnan electrostatic representation for charged (nano)particles regardless of the ratio between particle size and thickness of the operational electric Debye layer thickness [7]. This approximation necessarily fails for HNPs with radius 1 nm to 10 nm and practical salt concentrations in the range 1 mM to 100 mM. A consequence is that NICAD requires, for proton titration data fitting, the adjustment of a 'particle Donnan volume' that (i) exceeds the physical size of the particles and (ii) systematically increases with decreasing salt concentration, even in the absence of significant particle swelling [7,28,34-36]. Items (i) and (ii) are inconsistent from an electrostatic point of view and simply reflect the inapplicable electrostatic description given in NICAD for particles whose size does not significantly exceed the Debye layer thickness [7]. In line with these

observations, force is to recognize that a sound alternative to NICAD modelling for NPs charge evaluation is urgently needed.

Accordingly, in this work we elaborate a new approach for the analysis of NPs proton titration data where Poisson-Boltzmann theory for soft particle electrostatics is consistently implemented. The particle charge is evaluated from proper spatial integration of the local particle charge density defined by an isotherm reflecting the chemical binding of charge determining protons to ionogenic sites located at the particle surface and within the particle body volume, and corrected by local electrostatics retrieved from numerical solution to the nonlinear Poisson-Boltzmann equation valid for weakly to highly charged particles. Unlike NICAD, this framework is used to generate proton titration curves with a consistent account of particle size-dependent potential profile over the whole spectrum of Debye layer extension, *i.e.* from the thin to the thick double layer regime. A complete numerical package (that we make available for the community) combining a home-made FORTRAN program (named SPBT) for PB-based computations of particle electrostatics and charge, and a free module (called PEST) for optimized adjustment of the relevant chemical and electrostatic model parameters, is developed. The combined SPBT-PEST programs allow for (i) the automated and constrained reconstruction of measured proton titration curves *and* associated proton affinity spectra collected at different salt concentrations, and (ii) the evaluation of the relevant particle electrostatic and protolytic features.

The whole methodology is successfully tested for a range of HNPs particles whose titration data and size measurements are available in literature, and the performance of SPBT-PEST duo is further explicitly compared with that of NICAD. In detail, unlike NICAD [36], SPBT-PEST successfully reproduces the dependence of measured particle charge on pH and salt concentration for all HNPs tested, including those for which Donnan representation is not applicable. For HNPs whose size legitimates the applicability of Donnan potential profile, NICAD succeeds in reproducing the experimental data *albeit* at the cost of a 'particle Donnan volume' that is adjusted to values that exceed the physical volume of the particles, which is physically impossible [7,28,34,35]. In addition, SPBT-PEST properly recovers proton titration data for HNPs with maintaining a constant particle radius for all salt concentrations tested, which contrasts with the empirical adjustment of the NICAD 'particle Donnan volume' found to systemically increase with decreasing salt concentration [28,34-36]. We find that the chemical parameters pertaining to proton binding and proton affinity distribution, as retrieved from data modelling by SPBT-PEST and NICAD, may largely differ, especially so for the smallest HNPs where Donnan representation is not appropriate. This finding simply highlights the empirical electrostatic foundation of NICAD model and implications thereof in terms of particle charge estimation. NICAD may succeed to reproduce, quantitatively, experimental proton titration data even for particles whose size forbids *a priori* its application. It does so thanks to the adjustment of the 'particle Donnan volume', which artificially counterbalances the electrostatic deficiency of the NICAD model to achieve data fitting. As a support of this element, it is found that both the Donnan volume and the key chemical parameters involved in the model can vary by 100% depending on the reported form of the empirical NICAD equation that defines the dependence of

574 'particle Donnan volume' on medium salt concentration. In contrast, SPBT-PEST does not require the
575 adjustment of a 'particle Donnan volume' for fitting proton titration curves, recalling that this volume,
576 when relevant, necessarily identifies with the physical volume of the particle and the electrostatic potential
577 therein (the Donnan potential) is independent of position. The Donnan electrostatic potential
578 representation at the particle/solution interface is nothing else than the solution of the PB equation in the
579 limit of thin double layers. As such, SPBT-PEST bypasses the necessity by NICAD to recourse to a
580 questionable over-parameterisation of particle electrostatics to reproduce experimental data. Unlike
581 NICAD [22,28,25], the PB-based alternative we propose integrates consistently the intimate connection
582 between particle double layer potential, particle size and background electrolyte concentration.
583 We believe that the here-highlighted shortcomings of NICAD in its phenomenological representation
584 of particle electrostatics should be of concern for the community as NICAD, together with WHAM that
585 suffers from similar electrostatic approximations, constitutes a widely employed basis for computing *e.g.*
586 metal-to-humic thermodynamic complexation or addressing metal bioavailability in relation to toxicity
587 effects assessment. Unlike NICAD and WHAM, the PB theoretical framework developed in this study
588 can be extended to account *explicitly* for the presence of multivalent ions in solution [6], an option that is
589 particularly interesting for analysing particle charging behaviour in natural waters rich in divalent cations.
590 In addition, depending on the nature of particles considered, inhomogeneous particle structure
591 composition and gradients in dielectric permittivity between particle body and extraparticulate medium
592 can be easily implemented within the PB equation along the lines described elsewhere [39],[64]. Such
593 particle structure and electrostatic refinements may be valuable provided that independent measurements
594 targeting these aspects (*e.g.* diffusion neutron scattering and dielectric spectroscopy) are available to avoid
595 the adjustment of an ill-defined set of parameters when reconstructing particle proton titration curves.
596
597 **Supporting material. A.** Detailed description of the HNPs considered in this work, of their size
598 measurement and of the estimation of their molar mass. **B.** Details of the NICA-Donnan modelling
599 framework. **C.** Details of here-developed SPBT-PEST treatment of proton titration data and associated
600 proton affinity spectra. **D.** Evaluation of the initial estimates of the chemical parameters involved in eq 6.
601 **E.** Performance of SPBT-PEST in recovering HNPs proton titration and affinity spectra data. **F.**
602 Comparison between SPBT-PEST and NICAD reconstructions of proton titration data. Additional details
603 on the procedure outlined in **E** with step-by-step treated examples are provided in the form of a SPBT-
604 PEST user manual that is available on request together with the SPBT executable file.
605
606 This research did not receive any specific grant from funding agencies in the public, commercial, or not-
607 for-profit sectors.
608
609 ## References

610 [1] K.H. Tan, Humic Matter in Soil and the Environment: Principles and Controversies, 2nd Edition,
611 Crc Press-Taylor & Francis Group, Boca Raton, 2014. https://doi.org/10.1201/b17037.
612 [2] J. Buffle, Complexation Reactions in Aquatic Systems: An Analytical Approach, Prentice Hall,
613 1988.
614 [3] G.R. Aiken, D.M. McKnight, P. MacCarthy, R.L. Wershaw, Humic Substances in Soil, Sediment, and
615 Water: Geochemistry, Isolation, and Characterization, Wiley, 1985.

[4] E.M. Thurman, R.L. Malcolm, Preparative isolation of aquatic humic substances, Environ. Sci. Technol. 15 (1981) 463–466. https://doi.org/10.1021/es00086a012.
[5] E.M. Thurman, R.L. Wershaw, R.L. Malcolm, D.J. Pinckney, Molecular size of aquatic humic substances, Organic Geochemistry. 4 (1982) 27–35. https://doi.org/10.1016/0146-6380(82)90005-5.
[6] R.M. Town, J.F.L. Duval, H.P. van Leeuwen, The Intrinsic Stability of Metal Ion Complexes with Nanoparticulate Fulvic Acids, Environ. Sci. Technol. 52 (2018) 11682-11690. https://doi.org/10.1021/acs.est.8b02896.
[7] R.M. Town, H.P. van Leeuwen, J.F.L. Duval, Rigorous Physicochemical Framework for Metal Ion Binding by Aqueous Nanoparticulate Humic Substances: Implications for Speciation Modeling by the NICA-Donnan and WHAM Codes, Environ. Sci. Technol. 53 (2019) 8516-8532. https://doi.org/10.1021/acs.est.9b00624.
[8] H.P. van Leeuwen, J. Buffle, Chemodynamics of Aquatic Metal Complexes: From Small Ligands to Colloids, Environ. Sci. Technol. 43 (2009) 7175–7183. https://doi.org/10.1021/es900894h.
[9] J.F.L. Duval, Chemodynamics of metal ion complexation by charged nanoparticles: a dimensionless rationale for soft, core–shell and hard particle types, Phys. Chem. Chem. Phys. 19 (2017) 11802–11815. https://doi.org/10.1039/C7CP01750B.
[10] J.F.L. Duval, R.M. Town, H.P. van Leeuwen, Applicability of the Reaction Layer Principle to Nanoparticulate Metal Complexes at a Macroscopic Reactive (Bio)Interface: a Theoretical Study, J. Phys. Chem. C. 121 (2017) 19147-19161. https://doi.org/10.1021/acs.jpcc.7b04031.
[11] J.F.L. Duval, R.M. Town, H.P. van Leeuwen, Lability of Nanoparticulate Metal Complexes at a Macroscopic Metal Responsive (Bio)interface: Expression and Asymptotic Scaling Laws, J. Phys. Chem. C. 122 (2018) 6052-6065. https://doi.org/10.1021/acs.jpcc.7b11982.
[12] H.P. van Leeuwen, J.F.L. Duval, J.P. Pinheiro, R. Blust, R.M. Town, Chemodynamics and bioavailability of metal ion complexes with nanoparticles in aqueous media, Environ. Sci.: Nano. 4 (2017) 2108–2133. https://doi.org/10.1039/C7EN00625J.
[13] J. Marinsky, J. Ephraim, A Unified Physicochemical Description of the Protonation and Metal-Ion Complexation Equilibria of Natural Organic-Acids (humic and Fulvic-Acids) .1. Analysis of the Influence of Polyelectrolyte Properties on Protonation Equilibria in Ionic Media - Fundamental-Concepts, Environ. Sci. Technol. 20 (1986) 349–354. https://doi.org/10.1021/es00146a006.
[14] J. Ephraim, S. Alegret, A. Mathuthu, M. Bicking, R. Malcolm, J. Marinsky, A United Physicochemical Description of the Protonation and Metal-Ion Complexation Equilibria of Natural Organic-Acids (humic and Fulvic-Acids) .2. Influence of Polyelectrolyte Properties and Functional-Group Heterogeneity on the Protonation Equilibria of Fulvic-Acid, Environ. Sci. Technol. 20 (1986) 354–366. https://doi.org/10.1021/es00146a007.
[15] D.G. Kinniburgh, C.J. Milne, M.F. Benedetti, J.P. Pinheiro, J. Filius, L.K. Koopal, W.H. Van Riemsdijk, Metal Ion Binding by Humic Acid: Application of the NICA-Donnan Model, Environ. Sci. Technol. 30 (1996) 1687–1698. https://doi.org/10.1021/es950695h.
[16] C.J. Milne, D.G. Kinniburgh, W.H. van Riemsdijk, E. Tipping, Generic NICA−Donnan Model Parameters for Metal-Ion Binding by Humic Substances, Environ. Sci. Technol. 37 (2003) 958–971. https://doi.org/10.1021/es0258879.
[17] E. Tipping, WHAMC—A chemical equilibrium model and computer code for waters, sediments, and soils incorporating a discrete site/electrostatic model of ion-binding by humic substances, Computers & Geosciences. 20 (1994) 973–1023. https://doi.org/10.1016/0098-3004(94)90038-8.
[18] E. Tipping, Humic Ion-Binding Model VI: An Improved Description of the Interactions of Protons and Metal Ions with Humic Substances, Aquatic Geochemistry. 4 (1998) 3–47. https://doi.org/10.1023/A:1009627214459.
[19] L.K. Koopal, T. Saito, J.P. Pinheiro, W.H. Van Riemsdijk, Ion binding to natural organic matter: General considerations and the NICA–Donnan model, Colloids Surf. A: Physicochem. Eng. Asp. 265 (2005) 40–54. https://doi.org/10.1016/j.colsurfa.2004.11.050.

[20] L. Koopal, W. Tan, M. Avena, Equilibrium mono- and multicomponent adsorption models: From homogeneous ideal to heterogeneous non-ideal binding, Adv. Colloid Interface Sci. 280 (2020) 102138. https://doi.org/10.1016/j.cis.2020.102138.
[21] J.C.M. de Wit, W.H. Van Riemsdijk, L.K. Koopal, Proton Binding to Humic Substances .1. Electrostatic Effects, Environ. Sci. Technol. 27 (1993) 2005–2014. https://doi.org/10.1021/es00047a004.
[22] M.F. Benedetti, W.H. Van Riemsdijk, L.K. Koopal, Humic Substances Considered as a Heterogeneous Donnan Gel Phase, Environ. Sci. Technol. 30 (1996) 1805–1813. https://doi.org/10.1021/es950012y.
[23] H. Lyklema, Fundamentals of Interface and Colloid Science Volume Iv Particulate Colloids Introduction to Colloid Science, in: Fundamentals of Interface and Colloid Science, Vol Iv: Particulate Colloids, Elsevier Science Bv, Amsterdam, 2005.
[24] J.F.L. Duval, H.P. van Leeuwen, Electrokinetics of Diffuse Soft Interfaces. 1. Limit of Low Donnan Potentials, Langmuir 20 (2004) 10324–10336. https://doi.org/10.1021/la0400508.
[25] J.F.L. Duval, Electrokinetics of Diffuse Soft Interfaces. 2. Analysis Based on the Nonlinear Poisson−Boltzmann Equation, Langmuir 21 (2005) 3247–3258. https://doi.org/10.1021/la040108i.
[26] J. Overbeek, The Donnan Equilibrium, Prog. Biophys. Mol. Biol. 6 (1956) 58–84.
[27] M.J. Avena, L.K. Koopal, W.H. van Riemsdijk, Proton binding to humic acids: Electrostatic and intrinsic interactions, J. Colloid Interface Sci. 217 (1999) 37–48. https://doi.org/10.1006/jcis.1999.6317.
[28] C.J. Milne, D.G. Kinniburgh, E. Tipping, Generic NICA-Donnan model parameters for proton binding by humic substances, Environ. Sci. Technol. 35 (2001) 2049–2059. https://doi.org/10.1021/es000123j.
[29] E. Companys, J.L. Garces, J. Salvador, J. Galceran, J. Puy, F. Mas, Electrostatic and specific binding to macromolecular ligands - A general analytical expression for the Donnan volume, Colloid Surf. A-Physicochem. Eng. Asp. 306 (2007) 2–13. https://doi.org/10.1016/j.colsurfa.2007.01.016.
[30] J.F.L. Duval, K.J. Wilkinson, H.P. van Leeuwen, J. Buffle, Humic substances are soft and permeable: Evidence from their electrophoretic mobilities, Environ. Sci. Technol. 39 (2005) 6435–6445.
[31] J.F.L. Duval, H. Ohshima, Electrophoresis of Diffuse Soft Particles, Langmuir 22 (2006) 3533–3546. https://doi.org/10.1021/la0528293.
[32] T. Saito, L.K. Koopal, S. Nagasaki, S. Tanaka, Electrostatic potentials of humic acid: Fluorescence quenching measurements and comparison with model calculations, Colloid Surf. A-Physicochem. Eng. Asp. 347 (2009) 27–32. https://doi.org/10.1016/j.colsurfa.2008.10.038.
[33] J.P. Pinheiro, A.M. Mota, J.M.R. d'Oliveira, J.M.G. Martinho, Dynamic properties of humic matter by dynamic light scattering and voltammetry, Anal. Chim. Acta. 329 (1996) 15–24. https://doi.org/10.1016/0003-2670(96)00097-9.
[34] W.G. Botero, M. Pineau, N. Janot, R.F. Domingos, J. Mariano, L.S. Rocha, J.E. Groenenberg, M.F. Benedetti, J.P. Pinheiro, Isolation and purification treatments change the metal-binding properties of humic acids: effect of HF/HCl treatment, Environ. Chem. 14 (2018) 417–424. https://doi.org/10.1071/EN17129.
[35] N. Janot, J.P. Pinheiro, W.G. Botero, J.C.L. Meeussen, J.E. Groenenberg, PEST-ORCHESTRA, a tool for optimising advanced ion-binding model parameters: derivation of NICA-Donnan model parameters for humic substances reactivity, Environ. Chem. 14 (2016) 31–38. https://doi.org/10.1071/EN16039.
[36] D. Gondar, R. Lopez, S. Fiol, J.M. Antelo, F. Arce, Effect of soil depth on acid properties of humic substances extracted from an ombrotrophic peat bog in northwest Spain, Eur. J. Soil Sci. 56 (2005) 793–801. https://doi.org/10.1111/j.1365-2389.2005.00715.x.
[37] E. Rotureau, F. Thomas, J.F.L. Duval, Relationship between swelling and the electrohydrodynamic properties of functionalized carboxymethyldextran macromolecules, Langmuir 23 (2007) 8460–8473. https://doi.org/10.1021/la700427p.

[38] R. Zimmermann, D. Kuckling, M. Kaufmann, C. Werner, J.F.L. Duval, Electrokinetics of a Poly(N-isopropylacrylamid-co-carboxyacrylamid) Soft Thin Film: Evidence of Diffuse Segment Distribution in the Swollen State, Langmuir 26 (2010) 18169–18181. https://doi.org/10.1021/la103526b.
[39] J.F.L. Duval, Dynamics of metal uptake by charged biointerphases: bioavailability and bulk depletion, Phys. Chem. Chem. Phys. 15 (2013) 7873–7888. https://doi.org/10.1039/C3CP00002H.
[40] M. Nederlof, J.C.M. de Wit, W.H. van Riemsdijk, L.K. Koopal, Determination of Proton Affinity Distributions for Humic Substances, Environ. Sci. Technol. 27 (1993) 846–856. https://doi.org/10.1021/es00042a006.
[41] J.C.M. de Wit, W.H. van Riemsdijk, L.K. Koopal, Proton Binding to Humic Substances .2. Chemical Heterogeneity and Adsorption Models, Environ. Sci. Technol. 27 (1993) 2015–2022. https://doi.org/10.1021/es00047a005.
[42] J.F.L. Duval, R. Zimmermann, A.L. Cordeiro, N. Rein, C. Werner, Electrokinetics of Diffuse Soft Interfaces. IV. Analysis of Streaming Current Measurements at Thermoresponsive Thin Films, Langmuir 25 (2009) 10691–10703.
[43] U. Ascher, J. Christiansen, R. Russell, Collocation Software for Boundary-Value Odes, ACM Trans. Math. Softw. 7 (1981) 209–222. https://doi.org/10.1145/355945.355950.
[44] M. Moussa, C. Caillet, R.M. Town, J.F.L. Duval, Remarkable Electrokinetic Features of Charge-Stratified Soft Nanoparticles: Mobility Reversal in Monovalent Aqueous Electrolyte, Langmuir 31 (2015) 5656–5666. https://doi.org/10.1021/acs.langmuir.5b01241.
[45] J.F.L. Duval, C. Werner, R. Zimmermann, Electrokinetics of soft polymeric interphases with layered distribution of anionic and cationic charges, Current Opinion in Colloid & Interface Science 24 (2016) 1–12.
[46] M. Hosse, K.J. Wilkinson, Determination of electrophoretic mobilities and hydrodynamic radii of three humic substances as a function of pH and ionic strength, Environ. Sci. Technol. 35 (2001) 4301–4306. https://doi.org/10.1021/es010038r.
[47] T. Lenoir, A. Manceau, Number of Independent Parameters in the Potentiometric Titration of Humic Substances, Langmuir. 26 (2010) 3998–4003. https://doi.org/10.1021/la9034084.
[48] T. Lenoir, A. Matynia, A. Manceau, Convergence-Optimized Procedure for Applying the NICA-Donnan Model to Potentiometric Titrations of Humic Substances, Environ. Sci. Technol. 44 (2010) 6221–6227. https://doi.org/10.1021/es1015313.
[49] PESThomePage.org, (n.d.). http://www.pesthomepage.org/Home.php.
[50] M.J. Avena, A.W.P. Vermeer, L.K. Koopal, Volume and structure of humic acids studied by viscometry: pH and electrolyte concentration effects, Colloids Surf. A: Physicochem. Eng. Asp. 151 (1999) 213–224. https://doi.org/10.1016/S0927-7757(98)00504-4.
[51] L. Zurita, F. Carrique, A. Delgado, The Primary Electroviscous Effect in Silica Suspensions - Ionic-Strength and Ph Effects, Colloids Surf. A: Physicochem. Eng. Asp. 92 (1994) 23–28. https://doi.org/10.1016/0927-7757(94)02943-1.
[52] F. Chan, J. Blachford, D. Goring, Secondary Electroviscous Effect in a Charged Spherical Colloid, J. Colloid Interface Sci. 22 (1966) 378-+. https://doi.org/10.1016/0021-9797(66)90018-X.
[53] D. Megias-Alguacil, F.J. Arroyo, F. Carrique, A.V. Delgado, The electroviscous effect in ethylcellulose latex suspensions. Effect of ionic strength and correlation between theory and experiments, Colloid Polym. Sci. 278 (2000) 647–653. https://doi.org/10.1007/s003960000299.
[54] J.R.S. Martin, I. Bihannic, C. Santos, J.P.S. Farinha, B. Demé, F.A.M. Leermakers, J.P. Pinheiro, E. Rotureau, J.F.L. Duval, Structure of Multiresponsive Brush-Decorated Nanoparticles: A Combined Electrokinetic, DLS, and SANS Study, Langmuir 31 (2015) 4779–4790. https://doi.org/10.1021/acs.langmuir.5b00530.
[55] E. Balnois, K.J. Wilkinson, J.R. Lead, J. Buffle, Atomic force microscopy of humic substances: Effects of pH and ionic strength, Environ. Sci. Technol. 33 (1999) 3911–3917. https://doi.org/10.1021/es990365n.
[56] J.R. Lead, K.J. Wilkinson, E. Balnois, B.J. Cutak, C.K. Larive, S. Assemi, R. Beckett, Diffusion coefficients and polydispersities of the Suwannee River fulvic acid: Comparison of fluorescence

correlation spectroscopy, pulsed-field gradient nuclear magnetic resonance, and flow field-flow fractionation, Environ. Sci. Technol. 34 (2000) 3508–3513. https://doi.org/10.1021/es991195h.
[57] N.E. Palmer, R. von Wandruszka, Dynamic light scattering measurements of particle size development in aqueous humic materials, Fresenius J. Anal. Chem. 371 (2001) 951–954. https://doi.org/10.1007/s002160101037.
[58] A. Covington, H. Butikofer, M. Camoes, M. Ferra, M. Rebelo, Procedures for Testing Ph Responsive Glass Electrodes at 25, 37, 65 and 85-Degrees-C and Determination of Alkaline Errors up to 1 Mol Dm-3 Na+, K+, Li+, Pure Appl. Chem. 57 (1985) 887–898. https://doi.org/10.1351/pac198557060887.
[59] L.G. Sillen, A.E. Martell, Stability constants of metal-ion complexes, 2nd edition, The Chemical Society, London, 1964.
[60] W. Tan, J. Xiong, Y. Li, M. Wang, L. Weng, L.K. Koopal. Proton binding to soil humic and fulvic acids: Experiments and NICA-Donnan modeling. Coll. Surf. A: PhysicoChem. Eng. Aspects 436 (2013) 1152–1158. https://doi.org/10.1016/j.colsurfa.2013.08.010
[61] Y.Z. Kouhail, M.F. Benedetti, P.E. Reiller. Formation of mixed Eu(III)-CO3-fulvic acid complex: Spectroscopic evidence and NICA-Donnan modeling. Chem. Geology 522 (2019) 175–185. https://doi.org/10.1016/j.chemgeo.2019.05.032
[62] P. Lodeiro, C. Rey-Castro, C. David, E.P. Achterberg, J. Puy, M. Gledhill. Acid-base properties of dissolved organic matter extracted from the marine environment. Sci. Total Environ. 729 (2020) 138437. https://doi.org/10.1016/j.scitotenv.2020.138437
[63] V. Tsiridis, M. Petala, P. Samaras, S. Hadjispyrou, G. Sakellaropoulos, A. Kungolos. Interactive toxic effects of heavy metals and humic acids on *Vibrio fischeri*. Ecotox. Env. Safety 63 (2006) 158-167. https://doi.org/10.1016/j.ecoenv.2005.04.005
[64] J.F.L. Duval, J.P.S. Farinha, J.P. Pinheiro. Impact of Electrostatics on the Chemodynamics of Highly Charged Metal–Polymer Nanoparticle Complexes, Langmuir 29 (2013) 13821–13835. https://doi.org/10.1021/la403106m.

Figure captions.

Figure 1: Proton titration curves for FPHA (A) and corresponding proton affinity spectra (B) collected at three $NaNO_3$ electrolyte concentrations: 10 mM (Δ), 30 mM (◊) and 100 mM (o). Symbols: measurements. Dotted lines: SPBT-PEST modelling results. Adopted model parameters are listed in **Tables 1-2**. The charge is expressed in moles of equivalent charges per kg of FPHA material.

Figure 2: Proton titration curves for SRFA (A) and corresponding proton affinity spectra (B) collected at three $NaNO_3$ electrolyte concentrations (indicated). Symbols: measurements. Dotted lines: SPBT-PEST modelling results. Adopted model parameters are given in **Tables 1-2**. The charge is expressed in moles of equivalent charges per kg of SRFA material.

Tables.

Table 1: Comparison between HNPs specific volumes v_p derived in this work and model-generated Donnan volume V_D computed from the parameters reported in literature for NICAD modelling. Eq S3 and eq S4 given in **SM** specify the way V_D was estimated, *i.e.* either *via* the two-parameter (α, β) dependent or the one-parameter (b) dependent NICAD empirical equations that relates V_D to the logarithm of ionic strength. Initial estimates (superscript i in the Table) and refined values (superscript ii) of particle size r_p and molecular weight M_w by SPBT-PEST are further

indicated. Numbers between brackets correspond to κr_p values, recalling that Donnan potential-representation is strictly applicable for κr_p >>1.

HNPs type	r_p ($\times 10^{-9}$ m)	M_w (kg mol^{-1})	v_p (m^3 kg^{-1})	Donnan fitting parameters	Model-generated Donnan volume V_D (m^3 kg^{-1})		
				α,β for eq. S3 or b for eq. S4	100 mM	10 mM	1 mM
FPHA [34]	3.1 to 5.9*,[i] 5.0[ii]	19.2 to 23[i] 23 [ii]	0.0137	α=0.60±0.32 β=-0.27±0.05	0.0074 (5.20)	0.0138 (1.64)	0.0257 (0.52)
SRFA [28]	0.6 to 1.05 [i] 0.6[ii]	0.5 to 1.5[i] 0.545 [ii]	0.0010	b=0.87	0.0055 (0.60)	0.0407 (0.20)	0.3020 (0.06)
LFA [35]	1.9 to 3.6[i] 3.6[ii]	5.5 to 11[i] 10 [ii]	0.0118	b=0.35 ± 0.02	0.0004 (3.74)	0.0009 (1.18)	0.0019 (0.37)
				α=0.93±0.20 β=-0.27±0.05	0.0158 (3.74)	0.0295 (1.18)	0.0550 (0.37)
Hf:FA [36]	0.75 to 1.0[i] 1.0[ii]	0.5 to 1.5[i] 0.9 [ii]	0.0028	b=0.43	0.0007 (1.04)	0.0019 (0.33)	0.0052 (0.10)
Hf:HA [36]	0.75 to 1.0[i] 1.0[ii]	1.0 to 3.0[i] 1.8 [ii]	0.0014	b=0.34	0.0005 (1.04)	0.0010 (0.33)	0.0023 (0.10)

*Determined in this work by Scanned Stripping Chronopotentiometry (SSCP), see details in **SM** (**section A**, therein).

Table 2: SPBT-PEST optimized values of the chemical parameters involved in the Langmuir-Freundlich equation (eq 6) for the various HNPs types considered in this work. Indicated dispersions of the parameters correspond to the 95% confidence interval provided by PEST. The parameters are retrieved from SPBT-PEST and NICAD modelling of the proton titration curves measured at different salt reconstructions and reported in **Figures S6-S10** for the five HNPs samples of interest. SPBT-PEST and NICAD theoretical reconstructions of these proton titration data *versus* pH and salt concentration are also provided in **Figures S6-S10**.

HNPs type	*Model*	Q_{maxH1} (mol kg^{-1})	log $\overline{K}_{a1}$	m_{H1}	Q_{maxH2} (mol kg^{-1})	log $\overline{K}_{a2}$	m_{H2}
FPHA	SPBT-PEST	4.08 ± 0.02	4.26 ± 0.02	0.46 ± 0.01	1.39 ± 0.07	8.57 ± 0.09	0.59 ± 0.03
	NICAD/eq.S3 [34]	3.18 ± 0.92	3.65 ± 0.23	0.66	3.02 ± 2.4	8.07 ± 0.77	0.29
SRFA	SPBT-PEST	5.47 ± 0.06	3.20 ± 0.02	0.52 ± 0.01	1.0 ± 0.4	7.8 ± 0.2	0.5 ± 0.2
	NICAD/eq.S4 [28]	5.55	3.01	0.42	NA*	NA*	NA*
LFA	SPBT-PEST	3.79 ± 0.12	3.94 ± 0.03	0.52 ± 0.02	4.94 ± 0.10	8.5 ± 0.2	0.27 ± 0.01
	NICAD/eq.S4 [35]	2.8 ± 1.2	2.5 ± 0.2	0.62 ± 0.17	7.4 ± 2.5	7.4 ± 0.7	0.18 ± 0.06
	NICAD/eq.S3 [35]	5.1 ± 0.0	4.1 ± 0.1	0.41 ± 0.01	2.8 ± 0.0	8.6 ± 0.1	0.46 ± 0.02

Hf:FA	SPBT-PEST	4.35 ± 0.09	3.81 ± 0.01	0.91 ± 0.02	1.75 ± 0.06	7.1 ± 0.3	0.33 ± 0.01
	NICAD/eq.S4 [36]	5.0±0.01	2.29±0.01	0.44	0.94 ±0.03	6.85±0.02	0.59
Hf:HA	SPBT-PEST	3.00 ± 0.05	4.40 ± 0.02	0.83 ± 0.03	1.3 ± 0.2	7.5 ± 0.2	0.49 ± 0.05
	NICAD/eq.S4 [36]	3.44± 0.02	3.35 ± 0.01	0.46	0.64 ± 0.04	6.68 ± 0.03	0.88

NA (not available)*: NICAD fit was carried out only for site 1 type (*i.e.* carboxylic) due to the experimental data covering a reduced pH range (see Fig. 2)

SUPPORTING MATERIAL

Addressing the electrostatic component of protons binding to aquatic nanoparticles beyond the Non-Ideal Competitive Adsorption (NICA)-Donnan level: theory and application to analysis of proton titration data for humic matter.

José Paulo Pinheiro,[1] Elise Rotureau,[1] Jérôme F. L. Duval[1,*]

[1] Université de Lorraine, CNRS, Laboratoire Interdisciplinaire des Environnements Continentaux (LIEC), UMR 7360, Vandoeuvre-lès-Nancy, F-54000, France.

[*] Corresponding author: jerome.duval@univ-lorraine.fr
Tel: 00 33 3 72 74 47 20

This supporting material contains 12 pages, 6 equations, 18 references and 10 figures. It is organized as follows:

A. Detailed description of the HNPs considered in this work, of their size measurement and of the estimation of their molar mass.

B. Details of the NICA-Donnan modelling framework.

C. Details of here-developed SPBT-PEST treatment of proton titration data and associated proton affinity spectra.

D. Evaluation of the initial estimates of the chemical parameters involved in eq 6.

E. Performance of SPBT-PEST in recovering HNPs proton titration and affinity spectra data.

F. Comparison between SPBT-PEST and NICAD reconstructions of proton titration data.

A. Detailed description of the HNPs considered in this work, of their size measurement and of the estimation of their molar mass.

A1. FPHA particle type. FPHA sample was extracted from a peat sample collected in the Mogi river region of Ribeirão Preto, São Paulo State, Brazil [1], following the procedure recommended by IHSS for extraction and purification of organic matter [2]. Particle diffusion coefficient was measured by Scanning stripping chronopotentiometry (SSCP, see details below). The quadruplicate measurements yielded values of 5.2, 4.1, 5.9 and 4.7×10^{-11} $m^2\,s^{-1}$. Using Stokes-Einstein equation to convert diffusion coefficient into particle radius r_p, we obtained r_p = 4.5 nm and a 95% confidence interval of 3.1 to 5.9 nm. The FPHA sample was extracted from a tropical peat and measured particle size shows that it is a relatively large HNP material. In the literature, the closest sample we found is PPHA, for which molar masses of 23 kg mol^{-1} has been measured by equilibrium UV scanning ultracentrifugation [3]. Perminova *et al.* [4] reported number (M_n) and weight (M_w) average molecular weights of 6.4 and 19.2 kg mol^{-1}, respectively, by size exclusion chromatography on 8 peat humic substances samples.

Determination of FPHA diffusion coefficient by SSCP. Diffusion coefficient was determined using Cd(II) as a probe according to the procedure detailed by Pinheiro *et al.* [5] The experiments were carried out using an Ecochemie µAutolab III and a PGStat 12 in conjunction with a Metrohm 663 VA stand (Metrohm, Switzerland). The setup was controlled by the GPES 4.9 software from EcoChemie, the Netherlands. A three electrodes configuration was used, with a Hg thin film plated onto a rotating glassy carbon disk (2 mm diameter, Metrohm) serving as a working electrode, a GC rod counter electrode, and an Ag/AgCl reference electrode from World Precision Instruments DRIREF-5 (electrolyte leakage < 8×10^{-4} µL h^{-1}). SSCP experiments were carried out in 20 mL of 10 mM $NaNO_3$ solution with a Cd(II) concentration in the range 6 to 10×10^{-7} mol l^{-1} and a FPHA concentration in the range 8 to 10×10^{-5} kg l^{-1}. The adopted experimental conditions were: deposition time (t_d) 45 s, oxidizing current (I_s) 2×10^{-6} A applied until the potential reached -0.300 V with respect to Ag/AgCl reference electrode, rotation speed 1000 rpm. All solutions were purged for 15 min at the beginning of every experiment and for 20 s after each measurement (assisted by mechanical stirring of the rotating electrode). Measurements were performed for a range of deposition potentials, from the foot to the plateau of the SSCP wave, *i.e.* from -0.850 to -0.600 V for Cd(II).

A2. SRFA particle type. The Suwanee river fulvic acid (SRFA) is one of the International Humic Substances Society (IHSS) reference materials and probably the most studied HNP sample type. In 2001, Hosse and Wilkinson [6] measured SRFA diffusion coefficient by Fluorescence correlation spectroscopy (FCS) under different pH and ionic strength conditions and reported values between 2.1 and 2.6×10^{-10} $m^2\,s^{-1}$, which correspond to particle radius in the range 0.85 to 1.05 nm. De Wit *et al.* [7] reported a value of 0.6 nm, placing this material in the low end of the 1-2 nm range commonly reported for fulvic acids. Molar masses of 0.829 kg mol^{-1} and 0.545 kg mol^{-1} were reported for SRFA by Aiken *et al.* [8] and De

Wit *et al.* [7], respectively, while Her *et al.* [9] reported value of 1.116 kg mol^{-1} obtained by HPSEC/DOC and 1.385 kg mol^{-1} by HPSEC/UVA measurements.

A3. LFA particle type. LFA is a soil fulvic acid, extracted and purified from a podzol obtained in the Laurentian forest preserve of Laval University, Quebec, Canada [10]. The diffusion coefficients measured by voltammetry for the LFA range from 6×10^{-11} to 1.2×10^{-10} $m^2 s^{-1}$ at 10 mM ionic strength, corresponding to particle radius from 1.9 to 3.6 nm [11]. The LFA was extracted from a forest soil and its size is larger than that of SRFA. Shinozuka *et al.* [12] measured M_n of 9.7 and 11 kg mol^{-1} for Inogashira and Elliot soil fulvic acids by MALDI-TOF MS, while Perminova *et al.* [4] reported M_n of 5.5 kg mol^{-1} and M_w of 10.8 kg mol^{-1} averaged over 9 different samples.

A4. Hf:FA and Hf:HA particle types. Hf:FA and Hf:HA are the fulvic and humic acids extracted from the upper horizon (0-60 cm) of an ombrotrophic peat bog in Sierra del Buio, Northwest Spain. Pinheiro *et al.* [5] reported similar diffusion coefficients derived by FCS and SSCP, for both particle types with values in the range $2.3\text{-}2.8\times10^{-10}$ $m^2 s^{-1}$ at 10 and 100 mM ionic strength, which corresponds to r_p between 0.75 and 1.0 nm. This small particle size may be due to the fact that this material was extracted from the soil upper horizon where humification process is still recent. According to the authors [13], the collected sample contained reddish-brown fibric materials, while in the deeper horizons plant detritus was fully decomposed [13]. Hf:FA and Hf:HA particle radius indicates that they are a peculiar sample. Such a small radius is not compatible with large molar masses, thus we defined a low limit of 0.5 kg mol^{-1} for the FA and 1.0 kg mol^{-1} for the HA and fixed the higher limit at 1.5 and 3 kg mol^{-1} for the FA and HA samples, respectively in line with the M_w reported for small fulvic and humic NPs [7].

B. Details of the NICA-Donnan modelling framework.

NICA-Donnan model assumes *a priori* that the potential within the whole particle volume is constant (and takes the Donnan value ψ_D), and it further considers the accumulation of the only counterions within this volume and it neglects that of the coions that is however operational at sufficiently low particle charge and/or large electrolyte concentrations. In this model, cations accumulate inside the volume of (negatively charged) HNPs particles according to the Boltzmann accumulation factor

$$a_{i,D} = a_i exp(-z_i F\psi_D/RT) \quad \text{(S1)}$$

where a_i and z_i are the bulk activity and valence of cation *i*, respectively, *F* is the Faraday constant, *R* the gas constant and *T* is the temperature. Within the Donnan representation, the structural charge *Q* (in mol/kg of HNP material) located in the HNPs is neutralized by the cations, and the Donnan volume V_D (which identifies with the specific hydrodynamic volume of the particle in m^3/kg of HNP material) is defined by the electroneutrality equation:

$$Q/V_D + \sum_i z_i \left(a_{i,D} - a_i\right) = 0 \quad \text{(S2)}$$

Benedetti *et al.* [14] proposed an empirical relationship between V_D and the solution ionic strength (*I*) for HNPs:

$$\log V_D = \alpha + \beta \log I \quad \text{(S3)}$$

where α and β are parameters adjusted to match proton titration data and they depend on the nature of the HNP considered. The authors proposed later a 'simplification' of eq S3 with the following one-parameter dependent correlation between V_D and log I [15]

$$\log V_D = b(1 - \log I) - 1 \quad \text{(S4)}$$

Regarding the chemical component of the NICA equation,[16] it takes the form of a continuous equation that describes the competitive binding of cations to the HNP:

$$Q_{i,T} = \left(\frac{n_i Q_{\text{maxH1}}}{n_{H1}}\right) \frac{\left(\widetilde{K}_{i1} a_{i,D}\right)^{n_{i1}}}{\sum_i \left(\widetilde{K}_{i1} a_{i,D}\right)^{n_{i1}}} \frac{\left(\sum_i \left(\widetilde{K}_{i1} a_{i,D}\right)^{n_{i1}}\right)^{p_1}}{1+\left(\sum_i \left(\widetilde{K}_{i1} a_{i,D}\right)^{n_{i1}}\right)^{p_1}} +$$

$$\left(\frac{n_i Q_{\text{maxH2}}}{n_{H2}}\right) \frac{\left(\widetilde{K}_{i2} a_{i,D}\right)^{n_{i2}}}{\sum_i \left(\widetilde{K}_{i2} a_{i,D}\right)^{n_{i2}}} \frac{\left(\sum_i \left(\widetilde{K}_{i2} a_{i,D}\right)^{n_{i2}}\right)^{p_2}}{1+\left(\sum_i \left(\widetilde{K}_{i2} a_{i,D}\right)^{n_{i1}}\right)^{p_2}} \quad \text{(S5)}$$

where $Q_{i,T}$ is the total amount of species *i* bound to HNPs (mol kg^{-1}), $\widetilde{K}_{i1}$ and $\widetilde{K}_{i2}$ are the corresponding complexation parameters, n_{i1} and n_{i2} are the stoichiometric parameters relative to the binding of species *i* to the carboxylic (index 1) and phenolic (index 2) groups, respectively, Q_{maxH1} and Q_{maxH2} refer to the concentrations of carboxylic and phenolic groups, and p_1 and p_2 correspond to the intrinsic heterogeneity parameters of the carboxylic and phenolic binding sites. For the situation met in protolytic titrations experiments performed in inert $NaNO_3$, it can be legitimately assumed that the monovalent cations do not compete with the hydrogen ion [17], and eq S5 then reduces to

$$Q_{H,T} = Q_{\text{maxH1}} \frac{\left(\widetilde{K}_{H1} a_{H,D}\right)^{p_1 n_{H1}}}{1+\left(\widetilde{K}_{H1} a_{H,D}\right)^{p_1 n_{H1}}} + Q_{\text{maxH2}} \frac{\left(\widetilde{K}_{H2} a_{H,D}\right)^{p_2 n_{H2}}}{1+\left(\widetilde{K}_{H2} a_{H,D}\right)^{p_2 n_{H2}}} \quad \text{(S6)}$$

Eq S6 used to perform the reported NICAD analysis of the titration data collected for the samples of interest in this work is identical to eq 6 with the equivalences $m_{H1}=n_{H1}p_1$ and $m_{H2}=n_{H2}p_2$.

C. Details of here-developed SPBT-PEST treatment of proton titration data and associated proton affinity spectra.

This section describes in detail the optimization of the model parameters r_p, M_w, $\rho^{(s)}_{\text{maxH1}}$, $\rho^{(s)}_{\text{maxH2}}$ (or Q_{maxH1}, Q_{maxH2}), $\overline{K}_{a1}$, $\overline{K}_{a2}$, m_{H1} and m_{H2} to reproduce the raw proton titration data and the associated affinity spectra by coupling SPBT with PEST. The optimization procedure is further summarized in the flowchart displayed in **Figure S1** and briefly discussed below.

In the **first step** of the data treatment, an *input data* file containing the measured HNPs charge *Q* (in mol kg^{-1}) *vs.* pH at given solution ionic strength *I* and the associated proton affinity spectrum (d*Q*/dpH *vs.* pH) is created. This spectrum was computed using Matlab™ *via* cubic spline smoothing of the experimental *Q vs.* pH data and subsequent derivation of the splined data with respect to pH.

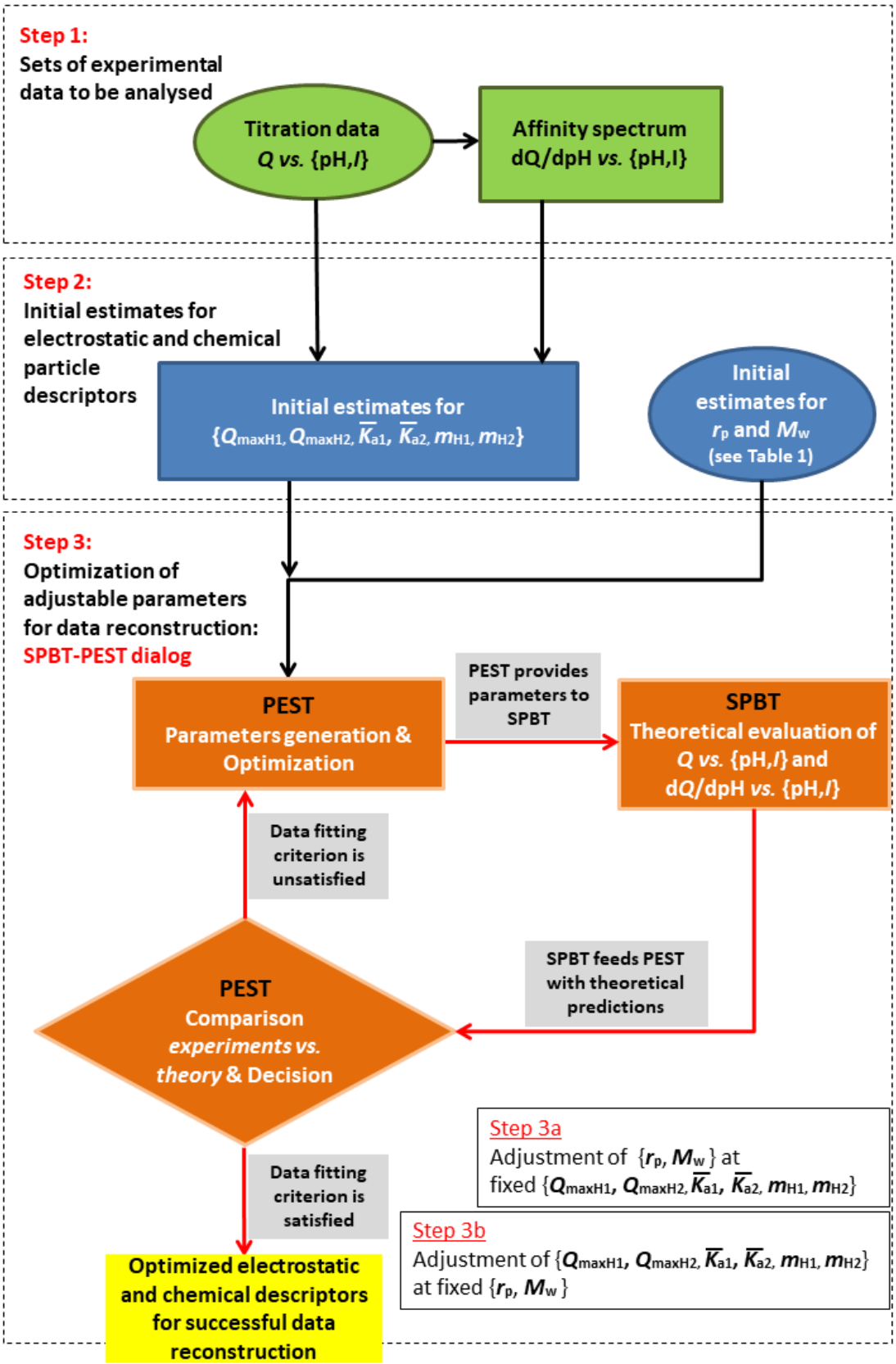

Figure S1: Flowchart detailing the procedure adopted for the reconstruction of proton titration data and proton binding affinity spectra, and for the evaluation of the chemical and electrostatic properties of HNPs. See details in the text.

The **second step** consists in establishing initial estimates for all parameters. As far as r_p and M_w are concerned, their respective estimates are listed in **Table 1** whereas those for Q_{maxH1}, Q_{maxH2}, m_{H1}, m_{H2}, $\overline{K}_{a1}$ and $\overline{K}_{a2}$ were evaluated from the proton titration curve Q *vs.* pH and the corresponding affinity spectrum dQ/dpH *vs.* pH measured at the largest electrolyte concentration (so as to minimize particle electrostatics contribution) along the lines detailed in **SM** (**section D**, **Figure S2**).

The back and forth communication between SPBT and PEST to achieve theoretical reconstruction of titration data takes place in a third step. First (step 3a in **Figure S1**), the *parameter template* file instructs PEST to fit r_p and M_w with the parameters Q_{maxH1}, Q_{maxH2}, m_{H1}, m_{H2}, $\overline{K}_{a1}$ and $\overline{K}_{a2}$ fixed to their respective initial estimates. PEST then creates the *input parameter* file and it calls for execution of SPBT that subsequently returns an *output* file containing the Q and dQ/dpH *versus* pH and I data generated for the set of parameters values given in the *parameter* file. PEST then reads this *output* file, computes the weighted sum Σ of squared differences between model-generated values and experimental data. Subsequently, PEST uses a Gauss-Marquardt-Levenberg algorithm to generate an updated set of values for the adjustable parameters (those provided in the *parameter template* file), and it informs SPBT to re-evaluate Q and dQ/dpH *versus* pH and I with this new set of parameters. PEST then reads the corresponding *output* file and compares the newly computed Σ with that obtained in the previous iteration. The SPBT-PEST programs duo iterates this procedure until the relative parameter variation is smaller than a prescribed value after execution of a number of iterations specified by the user. It is stressed in PEST manual [18] that a relative parameters variation lower than 1% after 3 successive iterations is a good compromise between accuracy and running time, and these criteria were therefore adopted in our procedure. Once this parameters optimization criterion is satisfied, the updated values of r_p and M_w are given by PEST in a *result* file that further contains the Q and dQ/dpH *vs.* pH and I theoretically generated by SPBT. In step 3b of **Figure S1**, SPBT-PEST duo resumes the full procedure detailed in step 3a *albeit* with now considering r_p and M_w as non-adjustable parameters with values given by those obtained at the end of step 3a, and with adjusting Q_{maxH1}, Q_{maxH2}, m_{H1}, m_{H2}, $\overline{K}_{a1}$ and $\overline{K}_{a2}$ to achieve Q and dQ/dpH *vs.* pH and I data fitting. This is done *via* modification of the *parameter template* file that indicates to PEST which parameters it should now adjust and which ones should be maintained constant all along the iterated fitting procedure. Further details on the above procedure with step-by-step treated examples are provided in the form of a SPBT-PEST fitting manual that is available on request together with the SPBT executable file.

D. Evaluation of the initial estimates of the chemical parameters involved in eq 6.

An example of the procedure followed to evaluate initial estimates of the chemical parameters involved in eq 6 is provided in **Figure S2** for FPHA for which proton titration data were published by Botero *et al.* [1] The raw data are presented in terms of charge equivalents per kg of humic matter *versus* pH. Titration data collected at large background electrolyte concentration (100 mM $NaNO_3$ in **Figure S2**)

are selected to minimize as much as possible the contribution of electrostatics to proton binding and thus to provide best initial estimates of the only chemical terms involved in eq 6.

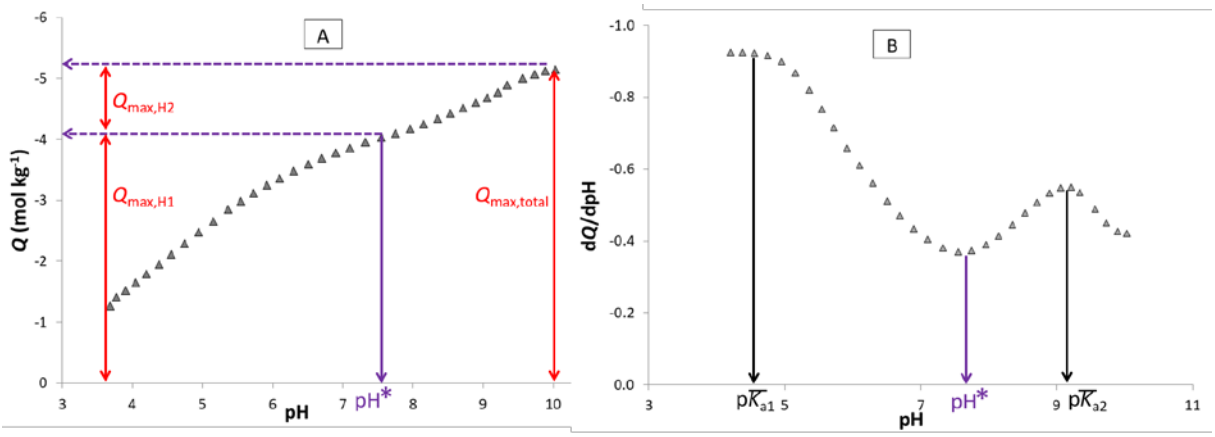

Figure S2: Illustration of the procedure followed for evaluation of the initial estimates of the chemical parameters involved in eq 6 from inspection of (A) proton titration data and (B) corresponding proton affinity spectrum. The data (symbols) refer to FPHA humic acids in 100 mM $NaNO_3$.

Initial estimates of Q_{maxH1}, Q_{maxH2}. The pH at which all carboxylic acids are titrated corresponds roughly to the onset of a plateau establishment for the particle charge Q with increasing pH. The clear location of this plateau is here necessarily impaired by the ongoing dissociation of the phenolic groups. For the lack of better, initial estimate of Q_{maxH1} is therefore read at the pH value marking a clear transition between dissociation features of carboxylic and phenolic HNP sites, *i.e.* at the pH value where the affinity spectrum displays a minimum with increasing pH (**Figure S2B**). Then, estimate for Q_{maxH2} can be obtained by simple difference between the maximum charge $Q_{\mathrm{max,total}}$ and Q_{maxH1} defined in **Figure S2**.

Initial estimates of $\mathrm{p}\overline{K}_{a1}$ and $\mathrm{p}\overline{K}_{a2}$. The two maxima in the proton affinity (**Figure S2B**) spectrum provides the desired initial estimates of $\mathrm{p}\overline{K}_{a1}$ and $\mathrm{p}\overline{K}_{a2}$.

Initial estimates of m_{H1} and m_{H2}. The parameters m_{H1} and m_{H2} correspond roughly to the half-height widths of the peaks detected for the carboxylic and phenolic groups in the proton affinity spectrum. A difficulty for their evaluation is that experimental affinity spectrum is generally incomplete in terms of the covered pH range (especially at low and high pH values), which explains why initial guessed values for m_{H1} and m_{H2} are commonly set to 0.5. For situations where optimized m_{H1} and m_{H2} significantly differ from 0.5, we restarted the overall SPBT-PEST fitting procedure with choosing as initial guessed values of m_{H1} and m_{H2} those obtained from the previous optimization scheme performed with adopting 0.5 as initial estimates.

E. Performance of SPBT-PEST in recovering HNPs proton titration and affinity spectra data.

The model parameters adopted for SPBT-PEST analysis of the charge and electrostatic descriptors of LFA, Hf:FA and Hf:HA are collected in **Tables 1-2** and we provide below in **Figure S3** (LFA),

Figure S4 (Hf:FA) and **Figure S5** (Hf:HA) the explicit confrontation between theoretical results and measured proton titration and corresponding affinity spectra.

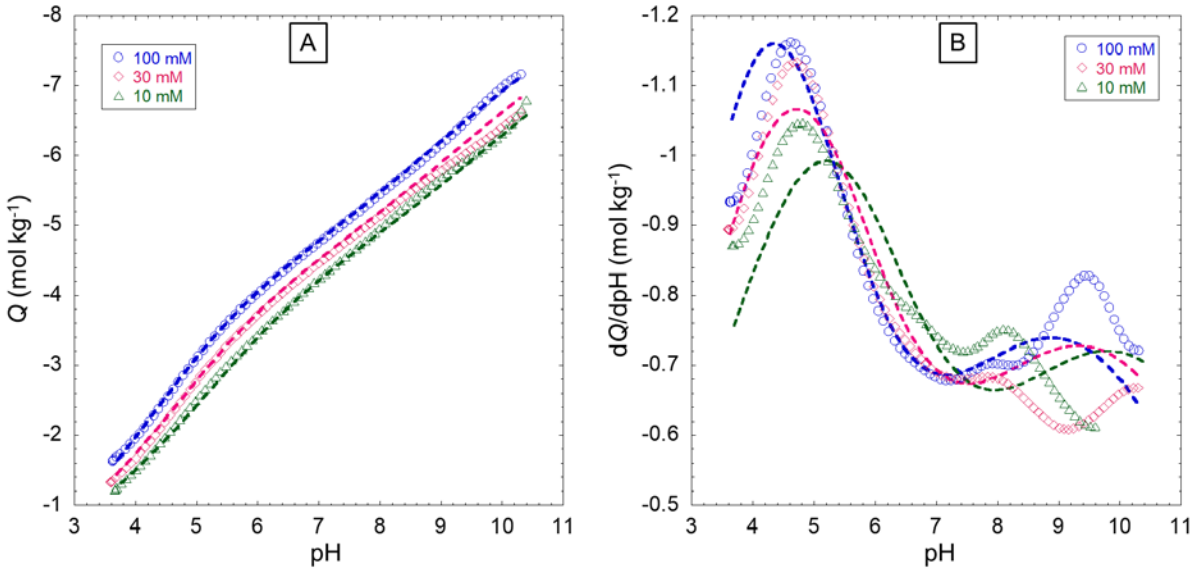

Figure S3: Proton titration curves for LFA (A) and corresponding proton affinity spectra (B) collected at three $NaNO_3$ electrolyte concentrations: 10 mM (Δ), 30 mM (◊) and 100 mM (o). Symbols: measurements. Dotted lines: SPBT-PEST modelling results. Model parameters are listed in **Tables 1-2**. The charge is expressed in moles of equivalent charges per kg of LFA material.

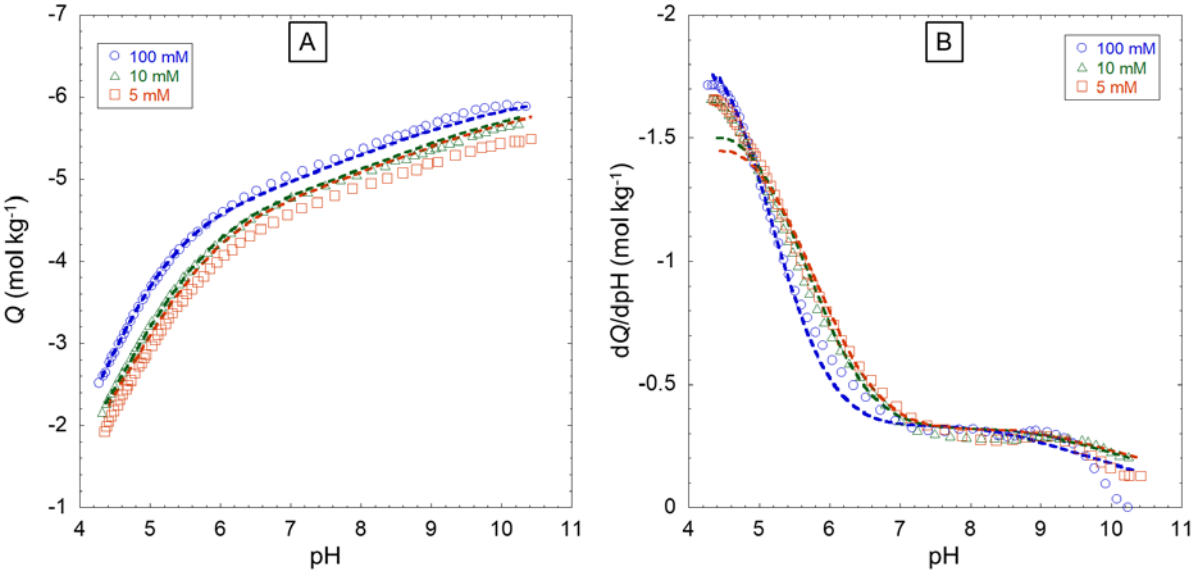

Figure S4: Proton titration curves for Hf:FA (A) and corresponding proton affinity spectra (B) collected at three $NaNO_3$ electrolyte concentrations (indicated). Symbols: measurements. Dotted lines: SPBT-PEST modelling results. Model parameters are listed in **Tables 1-2**. The charge is expressed in moles of equivalent charges per kg of Hf:FA material.

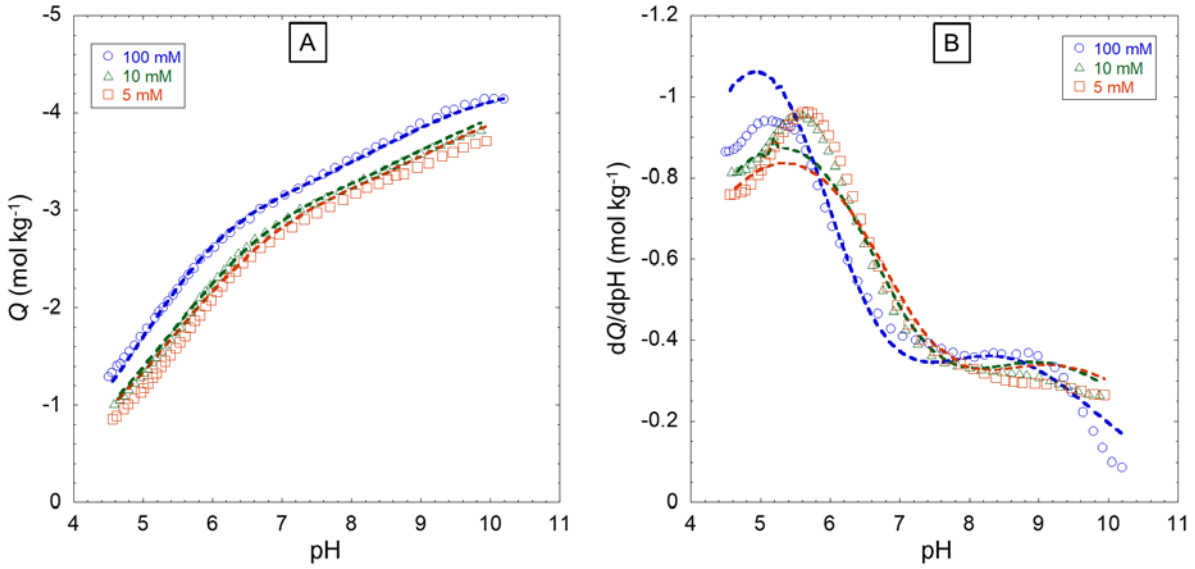

Figure S5: Proton titration curves for Hf:HA (A) and corresponding proton affinity spectra (B) collected at three $NaNO_3$ electrolyte concentrations (indicated) Symbols: measurements. Dotted lines: SPBT-PEST modelling results. Model parameters are listed in **Tables 1-2**. The charge is expressed in moles of equivalent charges per kg of Hf:HA material.

F. Comparison between SPBT-PEST and NICAD reconstructions of proton titration data.

For the sake of comparison, **Figures S6-S10** collect the experimental *Q vs*. pH and *I* data for the different HNPs samples of interest together with their theoretical fitting realized by NICAD and SPBT-PEST.

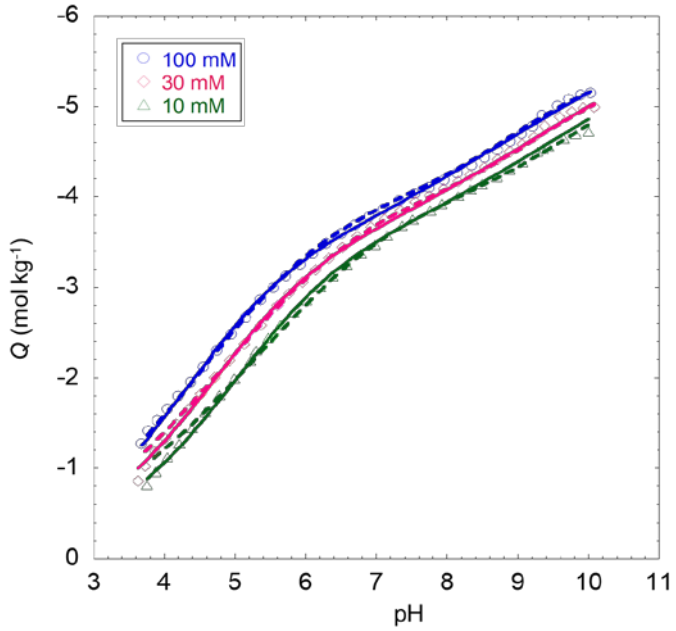

Figure S6: Proton titration curves for FPHA collected at three $NaNO_3$ electrolyte concentrations (indicated). Symbols: measurements. Dotted lines: SPBT-PEST modelling. Full lines: NICAD modelling. Model parameters are listed in **Tables 1-2**. The charge is expressed in moles of equivalent charges per kg of FPHA material.

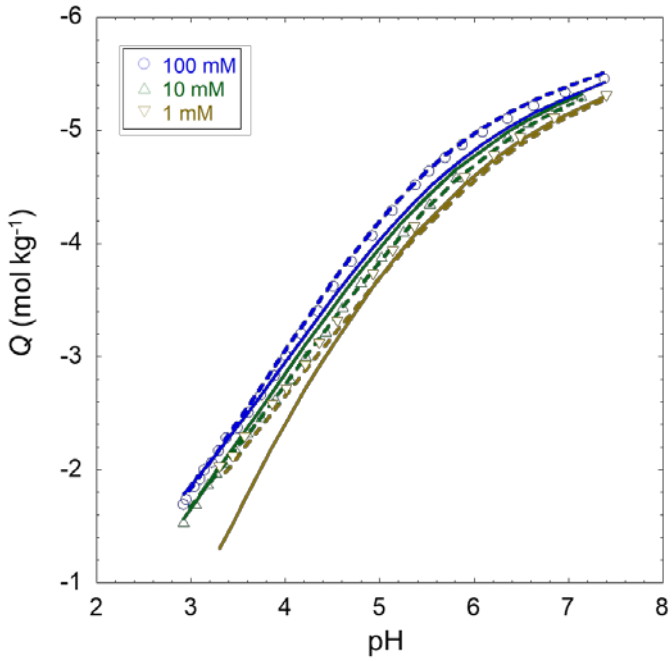

Figure S7: Proton titration curves for SRFA collected at three $NaNO_3$ electrolyte concentrations (indicated) Symbols: measurements. Dotted lines: SPBT-PEST modelling. Full lines: NICAD modelling. Model parameters are listed in **Tables 1-2.** The charge is expressed in moles of equivalent charges per kg of SRFA material.

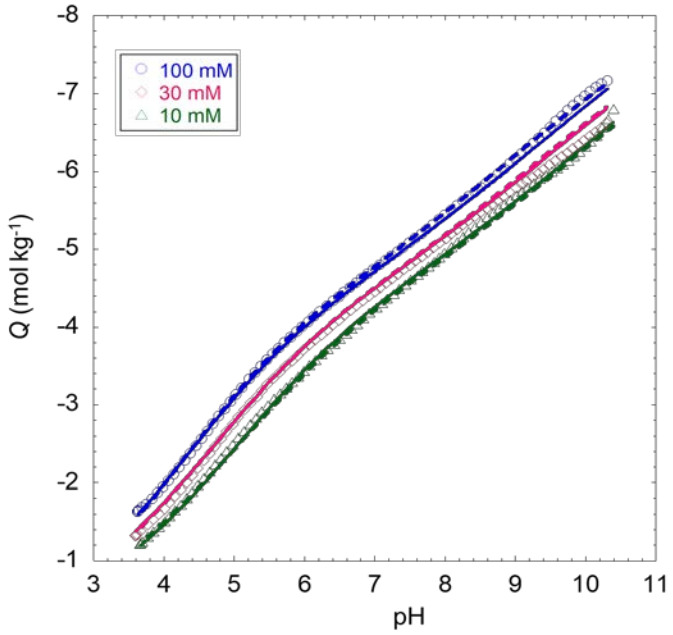

Figure S8: Proton titration curves for LFA collected at three $NaNO_3$ electrolyte concentrations (indicated). Symbols: measurements. Dotted lines: SPBT-PEST modelling. Full lines: NICAD modelling. Model parameters are listed in **Tables 1-2.** The charge is expressed in moles of equivalent charges per kg of LFA material.

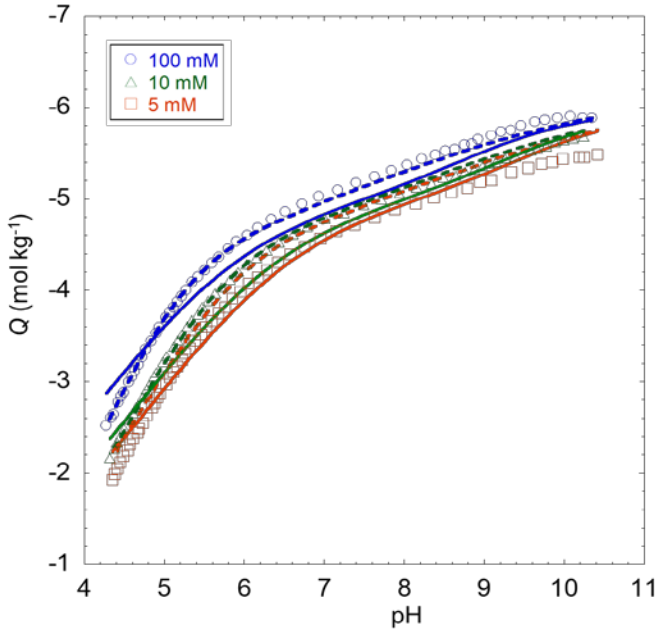

Figure S9: Proton titration curves for Hf:FA collected at three $NaNO_3$ electrolyte concentrations (indicated). Symbols: measurements. Dotted lines: SPBT-PEST modelling. Full lines: NICAD modelling. Model parameters are listed in **Tables 1-2**. The charge is expressed in moles of equivalent charges per kg of Hf:FA material.

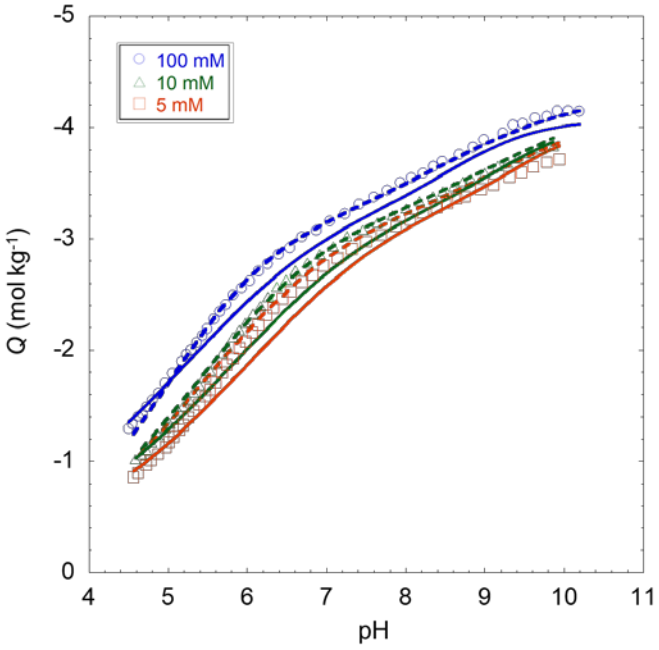

Figure S10: Proton titration curves for Hf:HA collected at three $NaNO_3$ electrolyte concentrations (indicated). Symbols: measurements. Dotted lines: SPBT-PEST modelling. Full lines: NICAD modelling. Model parameters are listed in **Tables 1-2**. The charge is expressed in moles of equivalent charges per kg of Hf:HA material.

References

[1] W.G. Botero, M. Pineau, N. Janot, R.F. Domingos, J. Mariano, L.S. Rocha, J.E. Groenenberg, M.F. Benedetti, J.P. Pinheiro, Isolation and purification treatments change the metal-binding properties of humic acids: effect of HF/HCl treatment, Environ. Chem. 14 (2018) 417–424. https://doi.org/10.1071/EN17129.

[2] E.M. Thurman, R.L. Malcolm, Preparative isolation of aquatic humic substances, Environ. Sci. Technol. 15 (1981) 463–466. https://doi.org/10.1021/es00086a012.

[3] M.J. Avena, A.W.P. Vermeer, L.K. Koopal, Volume and structure of humic acids studied by viscometry: pH and electrolyte concentration effects, Colloids Surf. A: Physicochem. Eng. Asp. 151 (1999) 213–224. https://doi.org/10.1016/S0927-7757(98)00504-4.
[4] I.V. Perminova, F.H. Frimmel, A.V. Kudryavtsev, N.A. Kulikova, G. Abbt-Braun, S. Hesse, V.S. Petrosyan, Molecular weight characteristics of humic substances from different environments as determined by size exclusion chromatography and their statistical evaluation, Environ. Sci. Technol. 37 (2003) 2477–2485. https://doi.org/10.1021/es0258069.
[5] J.P. Pinheiro, R. Domingos, R. Lopez, R. Brayner, F. Fiévet, K. Wilkinson, Determination of diffusion coefficients of nanoparticles and humic substances using scanning stripping chronopotentiometry (SSCP), Colloids and Surfaces A: Physicochemical and Engineering Aspects. 295 (2007) 200–208. https://doi.org/10.1016/j.colsurfa.2006.08.054.
[6] M. Hosse, K.J. Wilkinson, Determination of electrophoretic mobilities and hydrodynamic radii of three humic substances as a function of pH and ionic strength, Environ. Sci. Technol. 35 (2001) 4301–4306. https://doi.org/10.1021/es010038r.
[7] J.C.M. de Wit, W.H. Van Riemsdijk, L.K. Koopal, Proton Binding to Humic Substances .1. Electrostatic Effects, Environ. Sci. Technol. 27 (1993) 2005–2014. https://doi.org/10.1021/es00047a004.
[8] G.R. Aiken, D.M. McKnight, P. MacCarthy, R.L. Wershaw, Humic Substances in Soil, Sediment, and Water: Geochemistry, Isolation, and Characterization, Wiley, 1985.
[9] N. Her, G. Amy, D. Foss, J.W. Cho, Variations of molecular weight estimation by HP-size exclusion chromatography with UVA versus online DOC detection, Environ. Sci. Technol. 36 (2002) 3393–3399. https://doi.org/10.1021/es015649y.
[10] Z.-D. Wang, B. C. Pant, C. H. Langford, Spectroscopic and structural characterization of a Laurentian fulvic acid: notes on the origin of the color, Analytica Chimica Acta. 232 (1990) 43–49. https://doi.org/10.1016/S0003-2670(00)81224-6.
[11] J.P. Pinheiro, A.M. Mota, M.L.S.S. Goncalves, H.P. van Leeuwen, The pH effect in the diffusion coefficient of humic matter: influence in speciation studies using voltammetric techniques, Colloids Surf. A: Physicochem. Eng. Asp. 137 (1998) 165–170. https://doi.org/10.1016/S0927-7757(97)00306-3.
[12] T. Shinozuka, M. Shibata, T. Yamaguchi, Molecular Weight Characterization of Humic Substances by MALDI-TOF-MS, Journal of the Mass Spectrometry Society of Japan. 52 (2004) 29–32. https://doi.org/10.5702/massspec.52.29.
[13] D. Gondar, R. Lopez, S. Fiol, J.M. Antelo, F. Arce, Effect of soil depth on acid properties of humic substances extracted from an ombrotrophic peat bog in northwest Spain, Eur. J. Soil Sci. 56 (2005) 793–801. https://doi.org/10.1111/j.1365-2389.2005.00715.x.
[14] M.F. Benedetti, W.H. Van Riemsdijk, L.K. Koopal, Humic Substances Considered as a Heterogeneous Donnan Gel Phase, Environ. Sci. Technol. 30 (1996) 1805–1813. https://doi.org/10.1021/es950012y.
[15] D.G. Kinniburgh, C.J. Milne, M.F. Benedetti, J.P. Pinheiro, J. Filius, L.K. Koopal, W.H. Van Riemsdijk, Metal Ion Binding by Humic Acid: Application of the NICA-Donnan Model, Environ. Sci. Technol. 30 (1996) 1687–1698. https://doi.org/10.1021/es950695h.
[16] L.K. Koopal, T. Saito, J.P. Pinheiro, W.H. Van Riemsdijk, Ion binding to natural organic matter: General considerations and the NICA–Donnan model, Colloids Surf. A: Physicochem. Eng. Asp. 265 (2005) 40–54. https://doi.org/10.1016/j.colsurfa.2004.11.050.
[17] E. Iskrenova-Tchoukova, A.G. Kalinichev, R.J. Kirkpatrick, Metal Cation Complexation with Natural Organic Matter in Aqueous Solutions: Molecular Dynamics Simulations and Potentials of Mean Force, Langmuir. 26 (2010) 15909–15919. https://doi.org/10.1021/la102535n.
[18] PESThomePage.org, (n.d.). http://www.pesthomepage.org/Home.php.